The Existence and Stability of Spike Equilibria in the One-Dimensional Gray-Scott Model: The Pulse-Splitting Regime

Theodore Kolokolnikov*, Michael J. Ward†, Juncheng Wei‡

Abstract

The existence, stability, and pulse-splitting behavior of spike patterns in the one-dimensional Gray-Scott model on a finite domain is analyzed in the semi-strong spike-interaction regime. This regime is characterized by a localization of one of the components of the reaction near certain spike locations, while the other component exhibits a more global spatial variation across the domain. The method of matched asymptotic expansions is then used to construct k-spike equilibria in terms of a certain *core problem*. This core problem is studied numerically and asymptotically. For each integer $k \geq 1$, it is shown that there are two branches of k-spike equilibria that meet at a saddle-node bifurcation value. For small values of the diffusivity D of the second component, these saddle-node bifurcation points occur at approximately the same value. A combination of asymptotic and numerical methods is used to analyze the stability of these branches of k-spike equilibria with respect to both drift instabilities associated with the small eigenvalues and oscillatory instabilities of the spike profile. In this way, the key bifurcation and spectral conditions of Ei, Nishiura, Ueda [Japan. J. Indus. Appl. Math., 18, (2001)] believed to be essential for pulse-splitting behavior in a reaction-diffusion system are verified. By having verified these conditions, a simple analytical criterion for the occurrence of pulse-splitting is then formulated and confirmed with full numerical simulations of the Gray-Scott model. This criterion verifies a conjecture based on numerics and topological arguments reported in Doelman, Gardner, Kaper [this journal, 122 (1998)]. The analytical results are compared with previously obtained results for pulse-splitting behavior.

1 Introduction

We study the existence, stability, and pulse-splitting behavior of spike patterns in a certain asymptotic limit of the one-dimensional Gray-Scott (GS) model. This system, introduced for a continuously stirred reactor in [15], models an irreversible reaction involving two reactants in a gel reactor, where the reactor is maintained in contact with a reservoir of one of the two chemical species. In [30] (see also [20]), this system is written in nondimensional form as

$$v_t = \varepsilon^2 v_{xx} - v + Auv^2\,, \qquad -1 < x < 1\,, \quad t > 0\,; \qquad v_x(\pm 1, t) = 0\,, \tag{1.1a}$$

$$\tau u_t = Du_{xx} + (1-u) - uv^2 \qquad -1 < x < 1\,, \quad t > 0\,; \qquad u_x(\pm 1, t) = 0\,. \tag{1.1b}$$

Here $\varepsilon > 0$, $D > 0$, $\tau > 1$, and $A > 0$. The parameter A is referred to here as the feed-rate parameter. For various ranges of these parameters, (1.1) and its two-dimensional counterpart, are known to posses

*Department of Mathematics, University of British Columbia, Vancouver, Canada V6T 1Z2

†Department of Mathematics, University of British Columbia, Vancouver, Canada V6T 1Z2, (corresponding author)

‡Department of Mathematics, Chinese University of Hong Kong, New Territories, Hong Kong

a rich solution structure involving oscillating standing pulses, the propagation of traveling waves, pulse-replication behavior, and chaotic phenomena (cf. [5]–[9], [19], [24], [25], [28]–[30], [33], [35], [36], [37], [38], [39], [40], [43]). Self-replication of spots for the GS model was first observed numerically in [37]. Other early studies of pulse-splitting behavior for related systems were given in [19] (see Chapter 15 of [19]) and some of the references therein.

The dimensionless version (1.1) of the GS model, first introduced in [30], is particularly convenient in that it shows that, for $\varepsilon \ll 1$, the construction of equilibrium solutions depends only on the two parameters A and D, while the reaction-time constant $\tau > 1$ only influences the stability of these solutions. In the limit $\varepsilon \ll 1$, and for certain ranges of the other parameters, there are equilibrium solutions for v that consist of a sequence of spikes. The parameter D measures the effect of the finite domain and the strength of the inter-spike interactions. In this paper, we will assume that $D \gg O(\varepsilon^2)$ and $\varepsilon \ll 1$. In this regime, called the *semi-strong spike interaction regime*, spike patterns are such that v is localized near the spikes, while u varies more globally across the domain. This regime is to be contrasted with the weak interaction regime studied in [33], [35], [36], and [43], where $D = O(\varepsilon^2)$ and $\varepsilon \ll 1$.

In the semi-strong interaction limit there are three regimes for A where different behaviors occur; the *low feed-rate regime* $A = O(\varepsilon^{1/2})$, the *intermediate feed-rate regime* $O(\varepsilon^{1/2}) \ll A \ll O(1)$, and the *high feed-rate, or pulse-splitting, regime*, $A = O(1)$. These three regimes were first identified in [29] for (1.1), and in [7] in terms of another dimensionless version of the GS model. For the low feed-rate regime $A = O(\varepsilon^{1/2})$, it was shown in [9] and [20] that there is a saddle-node bifurcation structure of equilibrium k-spike patterns. In [20] a rigorous stability analysis of these solutions with respect to the large eigenvalues of order $\lambda = O(1)$ in the spectrum of the linearization showed that the stability properties depend intricately on A, D, τ, and k. Related work in the low-feed rate regime for a one-spike solution for the infinite-line problem was given in [29]. For the low feed-rate regime, the stability of k-spike equilibria with respect to the small eigenvalues of order $\lambda = O(\varepsilon^2)$ in the spectrum of the linearization was studied in [21].

For the intermediate regime, where $O(\varepsilon^{1/2}) \ll A \ll O(1)$, the stability of k-spike equilibria with respect to the large eigenvalues was first studied in [7] and [8] by deriving, and then analyzing, a certain nonlocal eigenvalue problem (NLEP). The analysis of this NLEP in [7] identifies parameter values at which the k-spike equilibria undergo a Hopf bifurcation. An alternative approach to study this NLEP was given in [20]. For a k-spike pattern, these results show that there are certain scaling laws in terms of a universal NLEP that determine the stability of equilibrium spike patterns with respect to the large eigenvalues of order $\lambda = O(1)$ in the spectrum of the linearization. Related results for a one-spike solution for the infinite-line problem were given in [29]. Regarding the small eigenvalues of order $\lambda = O(\varepsilon^2)$, it was shown in [21] that k-spike equilibria in the intermediate regime are all stable with respect to this class of eigenvalues when $\tau = O(1)$. However, in §5 of [21], it was shown that a small eigenvalue can become unstable, leading to a drift instability of a one-spike solution, when τ is asymptotically large as $\varepsilon \to 0$. This drift instability for the finite-domain problem, which results from a Hopf bifurcation, leads to an oscillatory behavior for the spike-layer location. In contrast, a monotonic drift instability for a one-spike solution for the infinite-line problem was found and analyzed in [28]. In Appendix A we summarize those main prior stability results for the intermediate regime that are relevant to the analysis in this paper.

The goal of this paper is to analyze the existence and stability of spike patterns for (1.1) in the pulse-splitting regime where $A = O(1)$. We will assume semi-strong spike interactions where $\varepsilon \ll 1$, $D \gg O(\varepsilon^2)$, and $\varepsilon A/\sqrt{D} \ll 1$. In this regime the equilibrium spike patterns again exhibit a saddle-node bifurcation structure. For the infinite-line problem, a one-spike equilibrium in this regime was constructed asymptotically in [30] and the saddle-node value was computed numerically. The existence of a saddle-node value for the infinite-line problem was proved using a topological shooting method in §6 of [7]. In [7] the saddle-node values for k-spike equilibria in the pulse-splitting regime were called "disappearance bifurcations", and were given numerically in Table 3 of §7.2 of [7]. A conjecture, based on numerical computations, for these saddle-node values was given in [7]. In §2 we construct equilibrium k-spike patterns in terms of a certain *core problem*. For the infinite-line problem, this core problem was introduced in [30] and was also given in a different form as the leading terms in equation (2.9) of [9]. Our approach extends the analysis in [30], [9], and [7], in two ways. Firstly, we incorporate the effect of the finite domain by matching the core solution to an appropriate outer expansion for the global variable u. This yields novel far-field boundary conditions that the core problem must satisfy. By analyzing this problem, we analytically verify the numerically-based conjecture of [7] for the saddle-node values. More specifically, we show formally in Principal Result 2.2 below that when $A = O(1)$ and $\varepsilon A/\sqrt{D} \ll 1$, there are no k-spike equilibria to (1.1) that match smoothly onto the intermediate regime solutions when $A > A_{pk}$, where

$$A_{pk} \equiv 1.347 \coth\left(\frac{1}{k\sqrt{D}}\right) . \tag{1.2}$$

The value 1.347 arises from the saddle-node bifurcation value for the core problem on the infinite line (cf. [30]), while the other term in (1.2) arises from our inner-outer matching of the core problem to the far field. Our second contribution to the equilibrium problem is that we analytically investigate qualitative properties of the solutions to the core problem including, asymptotic limiting shapes for the bifurcation branches and the analysis of a certain multi-bump transition structure. This mult-bump structure is important for pulse-splitting behavior. These results are given in Principal Results 3.1 and 3.2.

Next, we study the stability of the k-spike equilibria in the pulse-splitting regime $A = O(1)$ with respect to the small eigenvalues governing translational (drift) instabilities in the spike locations. In §4 we use an asymptotic matching analysis to analyze the stability of k-spike equilibria for $A = O(1)$ and $\varepsilon A/\sqrt{D} \ll 1$ with respect to the drift instabilities associated with eigenvalues of order $\lambda = O(\varepsilon)$. This stability analysis is significantly more intricate than that studied in [21] for the drift instability a one-spike solution in the intermediate regime. In Principal Result 4.2 we derive transcendental equations that the small eigenvalues satisfy. A central feature of this analysis is that, although the core problem can only be solved numerically, one can analytically calculate precise formulae for the small eigenvalues in terms of a single numerically-determined parameter related to the core problem. For $\tau \ll O(\varepsilon^{-1})$, Principal Result 4.3 shows that these eigenvalues are in the stable left half-plane for the equilibrium solution branch that merges onto the intermediate regime solution. In Principal Results 4.4 and 4.5 we show that when τ exceeds some threshold value in the regime $\tau = O(\varepsilon^{-1})$, a drift instability occurs as a result of a Hopf bifurcation. This leads to small-scale oscillations in the spike layer locations. The dominant instability is found to be a breathing-type instability (see Conjecture 4.6).

A related type of Hopf bifurcation has been analyzed in [16] and [26] for hyperbolic tangent-type interfaces associated with a two-component reaction diffusion system with bistable nonlinearities. Those analyses are based on the the SLEP (singular limit eigenvalue problem) method of [32]. Related oscillatory layer behavior for a certain three-component system has been studied numerically in [34].

In §5 we study the stability of k-spike equilibria in the pulse-splitting regime with respect to the large eigenvalues $\lambda = O(1)$, which govern oscillations in the spike amplitudes. A key observation is that the NLEP problem of the intermediate regime is not applicable in the pulse-splitting regime. Therefore, we study large eigenvalue instabilities numerically by formulating an eigenvalue problem and computing its spectrum by finite difference methods. For $\tau \ll O(\varepsilon^{-2})$, we show numerically that the equilibrium solution branch that merges onto the intermediate regime solutions is stable with respect to these eigenvalues, but that an instability due to a Hopf bifurcation in the spike profile can occur when $\tau = O(\varepsilon^{-2})$.

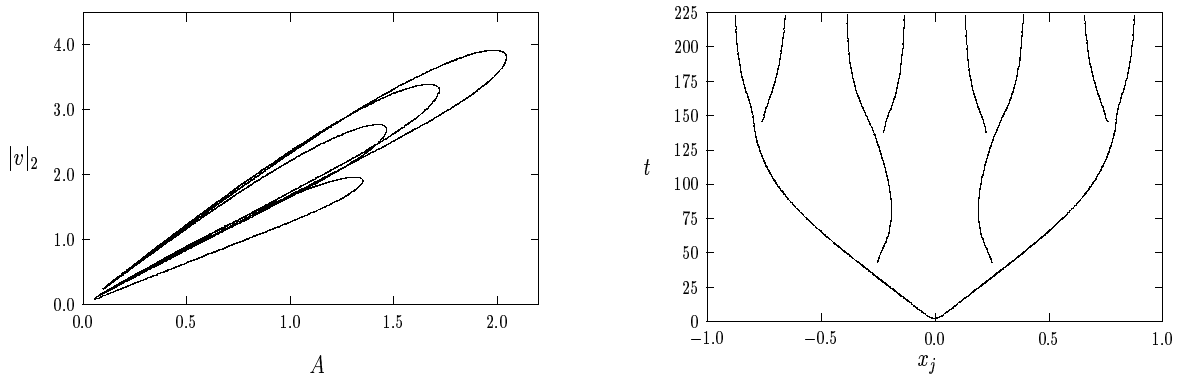

(a) $|v|_2$ versus A

(b) t versus x_j

Figure 1: Left figure: bifurcation diagram in the pulse-splitting regime $A = O(1)$ for k-spike solutions with $\varepsilon = 0.02$, $D = 0.1$, and $k = 1, \ldots, 4$. The fold point values for A increase with k. Right figure: trajectories of maxima of v showing pulse-splitting behavior when $\varepsilon = 0.01$, $D = 0.1$, $A = 2.4$, and $\tau = 2.0$.

The equilibrium results of §2 and §3, together with the stability results of §4 and §5, allow us to then verify the three main pulse-splitting conditions of [10] in the high-feed rate regime $A = O(1)$, and $\varepsilon A/\sqrt{D} \ll 1$. The first condition of [10] is that each k-spike equilibrium solution branch must have a fold-point, or saddle-node, bifurcation. Moreover, the fold points for each of these branches of equilibria must occur at approximately the same bifurcation value. This is the *lining-up property* of equilibria. For $D = 0.1$, in Fig. 1(a) we plot a bifurcation diagram of the L_2 norm of v, $|v|_2$, defined by

$$|v|_2 \equiv \left(\int_{-1}^{1} v^2 \, dx \right)^{1/2}, \tag{1.3}$$

versus A showing a saddle-node structure with an approximate lining-up property. The saddle-node bifurcation values in this figure are the values A_{pk} given in (1.2), that were also conjectured from numerical

computations in Table 3 of [7]. The second condition of [10] is that one of the branches of equilibria is unstable while the other is stable. When $\tau \ll O(\varepsilon^{-1})$ this stability condition is verified from the analysis and numerical computations of the small and large eigenvalues in §4 and §5, respectively. The final condition is that the spectrum of the linearization of the equilibrium solution at the fold point location has a *dimple-shaped* eigenfunction Φ_d, associated with a zero eigenvalue, for one of the components of the system. Such an eigenfunction is computed numerically in §5.

When the pulse-splitting conditions of [10] are satisfied, and when the bifurcation parameter is chosen to have a value slightly beyond the fold point value, it was argued in [35] that pulse-splitting should occur from a single localized initial pulse. The *ghost* of the dimple eigenfunction at the fold point value still influences the system for values of the bifurcation parameter slightly beyond this critical value. Similar *ghost* effects in other bifurcation settings have been well-studied, including dynamical hysteresis loops (cf. [14]), and delayed bifurcation effects caused by slowly varying control parameters (cf. [12]).

From our verification of the pulse-splitting criteria of [10], in §5 we then make a conjecture concerning the number of pulse-splitting events that will occur for (1.1) starting from a one-spike initial data. For $\tau \ll O(\varepsilon^{-1})$, $A = O(1)$, and $\varepsilon A/\sqrt{D} \ll 1$, Conjecture 5.1 predicts that a one-spike solution will undergo 2^{m-1} spitting events, and that the final equilibrium state will have 2^m spikes where, for some smallest integer $m > 0$, A lies in the interval

$$A_{p2^{m-1}} < A < A_{p2^m} \, . \tag{1.4}$$

Here A_{pk} is given in (1.2). In Fig. 1(b) we verify this conjecture for $\varepsilon = 0.01$, $D = 0.1$, $A = 2.4$, and $\tau = 2$. For these values, $A_{p4} = 2.045$ and $A_{p8} = 3.583$, so that $A_{p4} < A < A_{p8}$. In addition, $\tau = 2.0$ is below the drift instability threshold. Therefore, (1.4) correctly predicts the eight-spike final state in Fig. 1(b).

An important remark is that in our analysis we require that $\varepsilon A/\sqrt{D} \ll 1$. Therefore, the pulse-splitting that occurs in our regime is *distinctly different* from the pulse-splitting that occurs in the parameter regime of [10], [33], [35], [36], and [43], where $D = O(\varepsilon^2)$. When $D = O(\varepsilon^2)$, the inter-spike interactions become exponentially weak and there is a new core problem in the vicinity of each spike that involves a full balance of the terms in (1.1). In addition, pulse-splitting events occur only from the edge spikes (cf. [10]), in contrast to the pulse-splitting regime $A = O(1)$, with $\varepsilon A/\sqrt{D} \ll 1$, which involves a roughly simultaneous 2^m splitting of all the spikes in the sequence (see Fig. 1(b)).

In §6 we perform many numerical experiments to validate the asymptotic theory for pulse-splitting behavior, and we illustrate instabilities that can occur when τ is asymptotically large as $\varepsilon \to 0$. Finally, in §7 we carefully discuss the relationship between our results and certain results in the literature. In addition, we list some open problems.

2 Equilibria in the Pulse-Splitting Regime: $A = O(1)$

We now construct k-spike equilibria to (1.1) when $A = O(1)$. To do so, we first construct a symmetric one-spike equilibrium solution to (1.1) on the interval $-l < x < l$. Then, by setting $l = 1/k$, we obtain the result for a k-spike pattern for (1.1) on $-1 < x < 1$. The scalings for the inner region near $x = 0$ are suggested by the intermediate regime result (A.4a) of Appendix A. Therefore, we let $y = \varepsilon^{-1}x$, $v_i(y) = v(\varepsilon y)$,

$u_i(y) = u(\varepsilon y)$, and we expand the inner equilibrium solution for (1.1) as

$$v_i(y) = \varepsilon^{-1}\left(v_{i0} + \varepsilon v_{i1} + \cdots\right), \qquad u_i(y) = \varepsilon\left(u_{i0} + \varepsilon u_{i1} + \cdots\right). \tag{2.1}$$

We substitute (2.1) into (1.1), and collect powers of ε, to get inner problems on $-\infty < y < \infty$

$$v_{i0}'' - v_{i0} + A v_{i0}^2 u_{i0} = 0\,, \qquad D u_{i0}'' = u_{i0} v_{i0}^2\,, \tag{2.2a}$$

$$v_{i1}'' - v_{i1} + 2A v_{i0} u_{i0} v_{i1} = -A v_{i0}^2 u_{i1}\,, \qquad D u_{i1}'' = u_{i1} v_{i0}^2 + 2u_{i0} v_{i0} v_{i1} - 1\,. \tag{2.2b}$$

We look for even solutions with $u_{i0}'(0) = v_{i0}'(0) = u_{i1}'(0) = v_{i1}'(0) = 0$. The far-field conditions as $y \to \infty$ are that v_{i0} and v_{i1} tend to zero, whereas the conditions for u_{i0} and u_{i1} will be obtained by matching.

To determine the effect of the inner solution on the outer problem for u, we calculate $\varepsilon^{-1} u v^2$ in the sense of distributions. In this way, we obtain that the outer solution for u satisfies

$$D u_{xx} + (1 - u) = I_0 \delta(x) + \varepsilon I_1 \delta(x) + \cdots\,, \qquad -l < x < l\,, \tag{2.3a}$$

with $u_x(\pm l) = 0$, where $\delta(x)$ is the Dirac Delta function. Here I_0 and I_1 are defined by

$$I_0 \equiv \int_{-\infty}^{\infty} u_{i0} v_{i0}^2 \, dy\,, \qquad I_1 \equiv \int_{-\infty}^{\infty} \left(u_{i1} v_{i0}^2 + 2 v_{i0} v_{i1} u_{i0}\right) dy\,. \tag{2.3b}$$

Therefore, the solution to (2.3a) is

$$u(x) = 1 - I_0 G_l(x;0) - \varepsilon I_1 G_l(x;0) + \cdots\,. \tag{2.4}$$

Here $G_l(x;0)$ is the Green's function on $-l < x < l$ satisfying

$$D G_{lxx} - G_l = -\delta(x)\,, \quad -l < x < l\,; \qquad G_{lx}(\pm l;0) = 0\,; \qquad G_l(x;0) = \left(\frac{\theta_0}{2}\right) \frac{\cosh\left[(l - |x|)\theta_0\right]}{\sinh\left(l\theta_0\right)}\,. \tag{2.5}$$

To determine the conditions for matching to the inner solution, we expand $u(x)$ in (2.4) as $x \to 0^{\pm}$. Using (2.5) to calculate $G_l(0;0)$, $G_{lx}(0^{\pm};0)$, and $G_{lxx}(0;0)$, we then set $x = \varepsilon y$ to get

$$u \sim 1 - \frac{\theta_0}{2} I_0 \coth(l\theta_0) \pm \frac{\varepsilon y \theta_0^2}{2} I_0 - \frac{\varepsilon \theta_0}{2} I_1 \coth(l\theta_0) - \frac{\varepsilon^2 y^2 \theta_0^3}{4} I_0 \coth(l\theta_0) \pm \frac{\varepsilon^2 \theta_0^2 y}{2} I_1 + O(\varepsilon^3)\,. \tag{2.6}$$

We now match (2.6) to the inner solution u_i given in (2.1). Since $u_i = O(\varepsilon)$, the $O(1)$ term in (2.6) must vanish. This yields,

$$I_0 = \int_{-\infty}^{\infty} u_{i0} v_{i0}^2 \, dy = \frac{2}{\theta_0 \coth(l\theta_0)}\,. \tag{2.7}$$

Then, the εy term in (2.6) determines the far-field behavior of u_{i0}. In this way, we obtain that v_{i0} and u_{i0} satisfy (2.2a) subject to the far-field conditions

$$v_{i0} \to 0\,, \qquad u_{i0} \sim \frac{\theta_0 |y|}{\coth(l\theta_0)}\,, \qquad \text{as} \quad |y| \to \infty\,. \tag{2.8}$$

It is convenient to introduce new variables V and U defined by

$$v_{i0} = \sqrt{D} V\,, \qquad u_{i0} = \frac{1}{A\sqrt{D}} U\,. \tag{2.9}$$

Substituting (2.9) into (2.2a) and (2.8), we then obtain the leading-order *core problem*

$$V'' - V + V^2 U = 0\,, \qquad U'' = UV^2\,, \qquad 0 < y < \infty\,, \tag{2.10a}$$

$$V'(0) = U'(0) = 0\,; \qquad V \to 0\,, \qquad U \sim By\,, \qquad \text{as} \quad y \to \infty\,, \tag{2.10b}$$

where $U > 0$, $V > 0$, and

$$B \equiv \frac{A}{\coth(l\theta_0)}\,. \tag{2.11}$$

Before discussing some properties of (2.10), we continue with the matching to obtain a problem for v_{i1} and u_{i1}. In terms of the solution to (2.10), there is a constant $\chi = \chi(B)$ such that

$$U - By \to \chi\,, \qquad \text{as} \quad y \to \infty\,. \tag{2.12}$$

Then, the matching condition of the $O(\varepsilon)$ terms in the far-field behavior of the inner expansion for u and the outer expansion (2.6) determines I_1 in terms of χ by

$$I_1 = -\frac{2\chi}{A}\tanh(l\theta_0) = -\frac{2\chi}{B}\tanh^2(l\theta_0)\,. \tag{2.13}$$

Substituting (2.7) and (2.13) for I_0 and I_1, respectively, into the $O(\varepsilon^2)$ terms in the matching condition (2.6), we obtain that v_{i1} and u_{i1} satisfy (2.2b), subject to the far-field conditions

$$v_{i1} \to 0\,, \qquad u_{i1} \sim -\frac{y^2}{2D} - \frac{\chi}{BD}\tanh^2(l\theta_0)y \qquad \text{as} \quad y \to \infty\,. \tag{2.14}$$

It is then convenient to introduce the new variables V_1 and U_1 defined by

$$v_{i1} = AV_1\,, \qquad u_{i1} = \frac{1}{D}U_1\,. \tag{2.15}$$

Substituting (2.15) into (2.2b) and (2.14), we obtain that V_1 and U_1 satisfy

$$V_1'' - V_1 + 2VUV_1 = -V^2U_1\,, \qquad U_1'' = U_1V^2 + 2UVV_1 - 1\,, \qquad 0 < y < \infty\,, \tag{2.16a}$$

$$V_1'(0) = U_1'(0) = 0\,; \qquad V_1 \to 0\,, \qquad U_1 \sim -\frac{y^2}{2} - \frac{\chi}{B}\tanh^2(l\theta_0)y\,. \qquad \text{as} \quad y \to \infty\,. \tag{2.16b}$$

Here χ is defined by (2.12). Notice that U_1 is bounded uniformly in θ_0.

A two-term inner expansion is obtained by substituting (2.9) and (2.15) into (2.1). This yields,

$$v_i = \frac{\sqrt{D}}{\varepsilon}\left[V + \frac{\varepsilon A}{\sqrt{D}}V_1 + \cdots\right]\,, \qquad u_i = \frac{\varepsilon}{A\sqrt{D}}\left[U + \frac{\varepsilon A}{\sqrt{D}}U_1 + \cdots\right]\,. \tag{2.17}$$

Substituting (2.7) and (2.13) into (2.4), we get the two-term outer expansion for u, on $-l < x < l$,

$$u(x) = 1 - \frac{G_l(x;0)}{G_l(0;0)} + \frac{2\varepsilon\chi}{B}\tanh^2(l\theta_0)G_l(x;0)\,, \tag{2.18}$$

where $G_l(x;0)$ is given in (2.5).

We now make a few remarks. Firstly, the error terms in (2.17) show that (2.17) is valid when $\frac{\varepsilon A}{\sqrt{D}} \ll 1$. Notice that this condition is not valid for the weak interaction regime $D = O(\varepsilon^2)$ studied numerically in

[35], [36], and [43]. Hence, our analysis does not apply to this case. In this other pulse-splitting regime, where $A = O(1)$ and $D = O(\varepsilon^2)$, the inner solutions satisfy $v = O(1)$ and $u = O(1)$. Therefore, no asymptotic simplification of (1.1) is possible in the other pulse-splitting regime $A = O(1)$ and $D = O(\varepsilon^2)$. The second remark concerns the existence of asymmetric spike equilibria. Such patterns are possible when $u(l)$ is not monotone. However, (2.18) and (2.5) show that $u(l) \sim 1 - \operatorname{sech}(l\theta_0)$. Therefore, for $\varepsilon \ll 1$, $u(l)$ is monotone increasing, and so no asymmetric equilibria are possible.

To obtain a k-spike equilibrium solution we simply set $l = 1/k$, and extend $u(x)$ periodically across the interval from $-1 < x < 1$. This leads to our formally constructed equilibrium solution.

Principal Result 2.1: *Let $\varepsilon \to 0$, $A = O(1)$, $\varepsilon A/\sqrt{D} \ll 1$, and suppose that the core problem (2.10) has a solution. Then, the v-component for a k-spike equilibrium solution to (1.1) is given by*

$$v \sim \frac{\sqrt{D}}{\varepsilon} \sum_{j=1}^{k} \left(V\left[\varepsilon^{-1}(x - x_j)\right] + \frac{\varepsilon A}{\sqrt{D}} V_1\left[\varepsilon^{-1}(x - x_j)\right] + \cdots \right) . \tag{2.19a}$$

In the j^{th} inner region, where $|x - x_j| = O(\varepsilon)$ and $x_j = -1 + (2j-1)/k$, u satisfies

$$u \sim \frac{\varepsilon}{A\sqrt{D}} \left(U\left[\varepsilon^{-1}(x - x_j)\right] + \frac{\varepsilon A}{\sqrt{D}} U_1\left[\varepsilon^{-1}(x - x_j)\right] + \cdots \right) . \tag{2.19b}$$

Here V, U satisfy (2.10), while V_1, U_1 satisfy (2.16). In terms of the global Green's function $G(x; x_j)$ on $-1 < x < 1$, satisfying (A.3), the outer solution for u, valid for $|x - x_j| \gg O(\varepsilon)$ and $j = 1, \ldots, k$, is

$$u \sim 1 - \frac{1}{a_g}\left(1 - \frac{\varepsilon\chi\theta_0}{B}\tanh\left(\frac{\theta_0}{k}\right)\right) \sum_{j=1}^{k} G(x; x_j) , \qquad a_g \equiv \frac{\theta_0}{2}\coth\left(\frac{\theta_0}{k}\right) . \tag{2.19c}$$

2.1 The Core Problem

We now study the core problem (2.10) as a function of the parameter B. We first determine some analytical properties of (2.10). By integrating (2.10a) from $0 < y < \infty$, and using (2.10b), we get

$$\int_0^\infty V^2 U \, dy = \int_0^\infty V \, dy = B . \tag{2.20}$$

To parametrize the solution branches for (2.10), we define $U_0 \equiv U(0)$ and $V_0 \equiv V(0)$. Then, we multiply the V-equation in (2.10a) by V' and integrate the resulting equation in y. Using (2.10b), we then get

$$\frac{V_0^2}{2} + \int_0^\infty \frac{U}{3}\left[V^3\right]' \, dy = \frac{V_0^2}{2} - \frac{U_0 V_0^3}{3} - \int_0^\infty \frac{1}{3} V^3 U' \, dy = 0 . \tag{2.21}$$

This gives,

$$\int_0^\infty V^3 U' \, dy = V_0^2\left[\frac{3}{2} - U_0 V_0\right] . \tag{2.22}$$

By integrating the U-equation in (2.10a), and using $U'(0) = 0$, we obtain that $U' > 0$ on $0 < y < \infty$. Therefore, since the left hand-side of (2.22) is non-negative, we obtain a key inequality

$$0 < \gamma < \frac{3}{2} , \qquad \gamma \equiv U_0 V_0 . \tag{2.23}$$

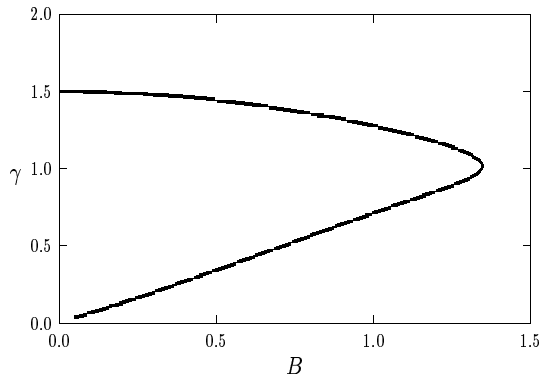

(a) γ versus B

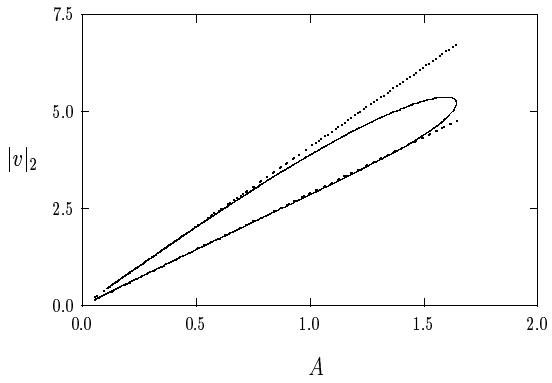

(b) $D = 0.75$

Figure 2: Left figure: plot of $\gamma = U_0 V_0$ versus B computed from the core problem (2.10). Right figure: plot of the norm $|v|_2$ given in (2.25) (solid curve) versus A for a one-spike solution when $D = 0.75$ and $\varepsilon = 0.02$. The dashed curves are the limiting asymptotic results (3.13) and (3.25).

As $\gamma \to 3/2$ from below, we show that there is a solution to (2.10) that has a single maximum for V and that matches onto the intermediate regime solution constructed in Principal Result 2.1.

The inequality (2.23) allows for a convenient parameterization of the solution branches of (2.10). Using the BVP solver COLSYS [2], we compute the numerical solution to (2.10) as a function of $\gamma = U_0 V_0$ for $0 < \gamma < 3/2$. For the starting point on the curve, where $\gamma \approx 3/2$, we use the intermediate regime solution given in (A.4a) of Appendix A. In this way, we obtain a function $B = B(\gamma)$ from (2.10b). In Fig. 2(a) we show that $B(\gamma)$ is multi-valued with $B \to 0$ as $\gamma \to 0$ and as $\gamma \to 3/2$. Numerically, we find that the maximum value B_c of B and the point γ_c where this maximum occurs is

$$B_c = 1.347\,, \qquad \gamma_c = 1.02\,. \tag{2.24}$$

This value agrees with that computed in [30] for the infinite-line problem. We refer to the upper branch in Fig. 2(a) as the *primary branch*, since it is this solution branch that merges smoothly as $B \to 0$ with the solution in the intermediate regime. The lower branch in this figure is referred to as the *secondary branch*.

In Fig. 2(b) we plot the norm $|v|_2$ versus $A = B\coth(\theta_0)$ for a one-spike solution when $D = 0.75$ and $\varepsilon = 0.02$. This norm is obtained by substituting (2.19a) into (1.3) to get

$$|v|_2 \sim \varepsilon^{-1/2}\sqrt{kD}\left(\int_{-\infty}^{\infty} V^2\,dy\right)^{1/2}\,. \tag{2.25}$$

The primary and secondary branches in the B, γ plane correspond to the upper and lower branches of Fig. 2(b), respectively. From (2.11) with $l = 1/k$, we then summarize our result concerning the existence of k-spike equilibrium solutions to (1.1) in the pulse-splitting regime.

Principal Result 2.2: *Let $\varepsilon \ll 1$, $A = O(1)$, and $\varepsilon A/\sqrt{D} \ll 1$. Then, there is no k-spike equilibrium solution to (1.1) that merges onto the intermediate regime equilibrium solution when*

$$A > A_{pk} \equiv 1.347 \coth\left(\frac{1}{k\sqrt{D}}\right) . \tag{2.26}$$

In §7 we remark that the value A_{pk}, derived here by asymptotic matching of inner and outer solutions, establishes the numerically-based conjecture of [7]. In Fig. 3(a) we plot the norm $|v|_2$, defined in (2.25), versus A for a k-spike solution with $k = 1, \ldots, 4$ when $\varepsilon = 0.02$ and $D = 0.75$. An identical plot is shown in Fig. 3(b) for $D = 0.1$. For this smaller value of D we observe an approximate lining-up property of k-spike equilibria. In these figures, the upper branches are the primary branches.

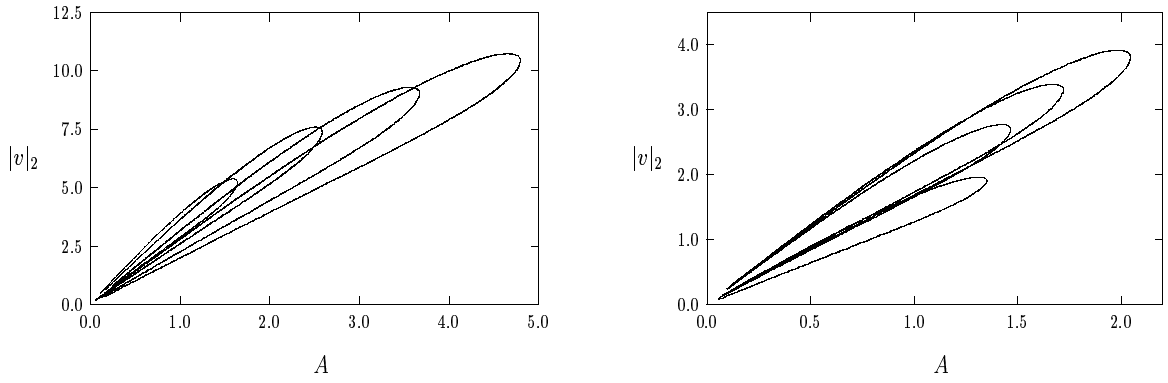

(a) $D = 0.75$ (b) $D = 0.1$

Figure 3: Left figure: plot of $|v|_2$ (solid curve) versus A for a k-spike solution with $k = 1, \ldots, 4$ when $\varepsilon = 0.02$ and $D = 0.75$. As k increases the value of A at the fold point increases. Right figure: same plot except that now $D = 0.1$. In this case, the fold points values are closer.

In Fig. 4(a) we plot the numerical solution to (2.10) at the point $\gamma = 1.26$ and $B \approx 1.03$ on the primary branch. For the point $\gamma = 0.326$ and $B \approx 0.476$ on the secondary branch, a similar plot is shown in Fig. 4(b). Notice that this latter solution for v has two bumps. This feature is studied below in §3. Although a rigorous proof of the shape of the $B = B(\gamma)$ curve and the behavior of the solution to the core problem (2.10) appears to be difficult, in §3 we give some insight into the behavior of the solutions near the extreme portions of this curve, where either $\gamma \to 0$ or $\gamma \to 3/2$. In [7] the existence of a fold point for the core problem (2.10), without the far-field behavior (2.11), was proved by a topological shooting argument.

3 Asymptotics of the Core Problem

We now study the limiting behavior of the core problem (2.10). We first study the limiting behavior of the primary branch where $\gamma \to 3/2$ from below. In this limit we have that $U(0) \equiv U_0 \gg 1$, and so we

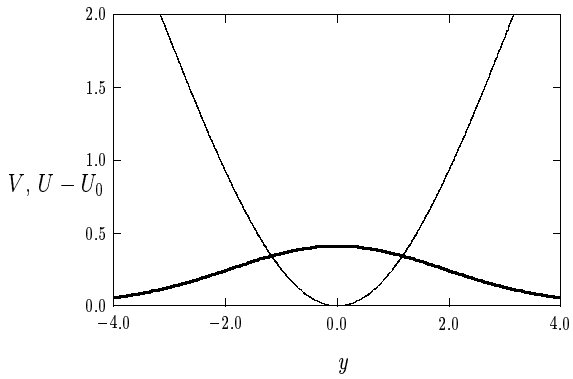

(a) Primary branch: $\gamma = 1.263$, $B \approx 1.03$

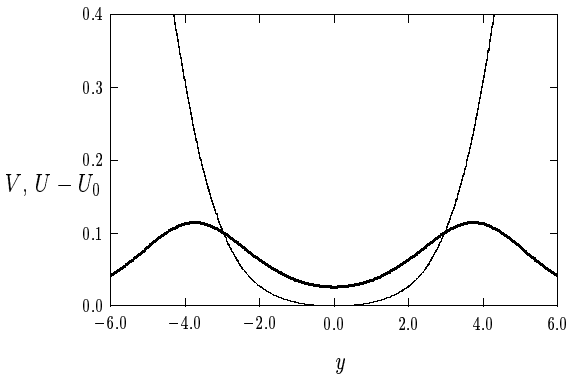

(b) Secondary branch: $\gamma = 0.326$, $B \approx 0.476$

Figure 4: Plots of the numerical solution to the core problem on either side of the fold point at $B = B_c = 1.347$ and $\gamma = \gamma_c = 1.02$. The heavy solid curves are V, while the solid curves are $U - U_0$.

introduce a small parameter δ by $\delta = 1/U_0$. This suggests that $U = O(\delta^{-1})$ and $V = O(\delta)$ in the core region. Therefore, in this limit, we expand the solution to (2.10) in terms of δ as

$$V = \delta \left(v_0 + \delta^2 v_1 + \cdots \right) , \qquad U = \delta^{-1} u = \delta^{-1} \left(u_0 + \delta^2 u_1 + \cdots \right) , \qquad \text{with} \quad u(0) = 1 . \tag{3.1}$$

Our choice of δ enforces that $u_0(0) = 1$ and $u_j(0) = 0$ for $j \geq 1$. Since $\int_0^\infty V \, dy = B$ from (2.20), the expansion (3.1) yields that $B = O(\delta)$. Hence, we write $B = \delta B_0$. Substituting (3.1) into (2.10), and collecting powers of δ, we obtain the leading-order problem

$$v_0'' - v_0 + v_0^2 u_0 = 0 , \qquad u_0'' = 0 , \tag{3.2}$$

with $v_0'(0) = 0$, $u_0(0) = 1$, and $v_0 \to 0$, $u_0' \to 0$ as $y \to \infty$. Therefore, $u_0(y) = 1$ and $v_0(y) = w(y)$, where w satisfies (A.2). From collecting terms of order $O(\delta^2)$, we obtain that v_1 and u_1 satisfy

$$L v_1 \equiv v_1'' - v_1 + 2 w v_1 = -w^2 u_1 , \quad 0 < y < \infty ; \qquad v_1'(0) = 0 , \quad v_1 \to 0 , \quad \text{as} \quad y \to \infty , \tag{3.3a}$$

$$u_1'' = w^2 , \quad 0 < y < \infty ; \qquad u_1'(0) = 0 , \quad u_1(0) = 0 , \quad u_1' \to B_0 , \quad \text{as} \quad y \to \infty . \tag{3.3b}$$

By integrating (3.3b) over $0 < y < \infty$, we get that $B_0 = \int_0^\infty w^2 \, dy = 3$.

Next, we multiply (3.3a) by w' and integrate over y. Since $L w' = 0$ and $w'(0) = v_1'(0) = 0$, we get

$$\int_0^\infty w' L v_1 \, dy = w''(0) v_1(0) = - \int_0^\infty w^2 w' u_1 \, dy . \tag{3.4}$$

Integrating the last term in (3.4) by parts, and noting that $u_1(0) = 0$, we get

$$w''(0) v_1(0) = \frac{1}{3} \int_0^\infty w^3 u_1' \, dy . \tag{3.5}$$

To calculate $v_1(0)$, we must determine $u_1'(y)$. To do so, we substitute $w(y) = \frac{3}{2}\mathrm{sech}^2(y/2)$ and $w^2 = w - w''$ directly into (3.3b) to obtain

$$u_1'' = w - w'' = \frac{3}{2}\mathrm{sech}^2(y/2) - w'' . \tag{3.6}$$

Integrating this equation twice, and using $u_1'(0) = 0$, $u_1(0) = 0$, we readily derive

$$u_1(y) = 6\ln\left[\cosh\left(\frac{y}{2}\right)\right] - \frac{3}{2}\mathrm{sech}^2\left(\frac{y}{2}\right) + \frac{3}{2} . \tag{3.7}$$

To determine $v_1(0)$, we integrate (3.6) once to get

$$u_1' = 3\tanh\left(\frac{y}{2}\right) - w' = -\frac{3w'}{w} - w' . \tag{3.8}$$

Finally, substituting (3.8) into (3.5), integrating the resulting expression by parts, and using the explicit form of w, we obtain

$$v_1(0) = \frac{1}{3w''(0)}\int_0^\infty \left(-3w^2w' - w'w^3\right) dy = \frac{1}{3w''(0)}\left[w^3(0) + \frac{w^4(0)}{4}\right] = -\frac{33}{16} . \tag{3.9}$$

Since $\gamma \equiv U_0V_0$, (3.1) yields $\gamma = w(0) + \delta^2 v_1(0)$. We summarize the result in the following statement:
Principal Result 3.1: *Let $\delta = 1/U_0 \ll 1$. Then, along the primary branch, the core problem (2.10) has a solution where $\gamma \to 3/2$ from below as $\delta \to 0$. This solution is given asymptotically by*

$$V \sim \delta\left(w(y) + \delta^2 v_1(y) + \cdots\right) , \qquad U \sim \delta^{-1}\left(1 + \delta^2 u_1(y) + \cdots\right) , \tag{3.10a}$$

where $w(y)$ satisfies (A.2). Here $u_1(y)$ is given in (3.7), and the local behavior for the $B = B(\gamma)$ curve is

$$B \sim 3\delta , \quad \gamma \equiv U_0V_0 \sim \frac{3}{2} - \frac{33}{16}\delta^2 , \quad \delta \ll 1 ; \qquad \gamma \equiv U_0V_0 \sim \frac{3}{2} - \frac{11B^2}{48} , \quad B \ll 1 . \tag{3.10b}$$

This limiting solution makes a smooth transition to the intermediate regime inner solution given in (A.4a) of Appendix A. To show this, we use $B \sim 3\delta$ and (2.11) to calculate δ in terms of A as

$$A = 3\delta\coth\left(\frac{\theta_0}{k}\right) . \tag{3.11}$$

Substituting the leading terms of (3.10a) into the leading terms of (2.17), we obtain for $\delta \ll 1$, that

$$v_i \sim \frac{A\sqrt{D}w}{3\varepsilon\coth(\theta_0/k)} , \qquad u_i \sim \frac{3\varepsilon\coth(\theta_0/k)}{A^2\sqrt{D}} , \tag{3.12}$$

which agrees with (A.4a). For $\delta \ll 1$, we can use $V \sim \delta w$, to calculate the norm in (2.25) as

$$|v|_2 \sim \varepsilon^{-1/2}\sqrt{kD}\left(\int_{-\infty}^{\infty} V^2\, dy\right)^{1/2} \sim \frac{A\varepsilon^{-1/2}\sqrt{6kD}}{3\coth(\theta_0/k)} . \tag{3.13}$$

This result also agrees asymptotically with the intermediate regime norm (A.5).

For the secondary solution branch in the B, γ parameter plane, we now construct an asymptotic solution to the core problem (2.10) where $\gamma \equiv U_0 V_0 \to 0$ from above. From (2.10a), we first observe that $V''(0) < 0$ when $\gamma > 1$, and $V''(0) > 0$ when $0 < \gamma < 1$. Therefore, for values of γ just below $\gamma = 1$, the solution for V starts to have a dimple at the origin. As γ is decreased further, this dimple becomes more pronounced, and as $\gamma \to 0$ the solution to (2.10) begins to look like two spikes symmetrically placed about the origin. This was illustrated in Fig. 4(b) for $\gamma = 0.326$ where $B \approx 0.476$. It is remarkable that the fold point value $\gamma_c = 1.02$, given in (2.24), occurs at almost the same value as where V first begins to exhibit a dimple. Therefore, as $\gamma = U_0 V_0 \to 0$, we expect that the core solution splits into two disjoint spikes.

To analyze this regime, we label $\delta = 1/U_0$, with $U_0 \equiv U(0)$, except that now we make a two-spike approximation for V with spikes located at $y = y_1 > 0$ and $y = -y_1$. As $\delta \to 0$, we will show that $y_1 \sim -\ln \delta \gg 1$. Therefore, the separation between the spikes grows logarithmically for $\delta \ll 1$. The analysis below to calculate y_1 is related to the analytical construction of multi-bump solutions to the Gierer-Meinhardt model (cf. [13]) given in [4]. We look for a two-bump solution to (2.10) in the form

$$V = \delta\,(w_1 + w_2 + R + \cdots)\,, \qquad U = \delta^{-1} u = \delta^{-1}\left(1 + \delta^2 u_1 + \cdots\right)\,, \qquad \text{with} \quad u_1(0) = 0\,. \tag{3.14}$$

Here we have labelled $w_1(y) \equiv w(y - y_1)$ and $w_2(y) \equiv w(y + y_1)$. Substituting (3.14) into (2.10), and assuming that $R \ll 1$, we obtain that u_1 and the residual R satisfy

$$LR \equiv R'' - R + 2(w_1 + w_2)R = -2w_1 w_2 - \delta^2\left(w_1^2 + w_2^2 + 2w_1 w_2\right) u_1\,, \quad -\infty < y < \infty\,, \tag{3.15a}$$

$$u_1'' = w_1^2 + w_2^2 + 2w_1 w_2\,, \qquad -\infty < y < \infty\,, \tag{3.15b}$$

with $u_1'(0) = 0$. Notice that R is small when the bumps are widely separated. In particular, when $y_1 = O(-\ln \delta)$, the two terms on the right hand-side of (3.15a) are both of order $O(\delta^2)$.

To determine y_1 we use a solvability condition. Assuming well-separated spikes so that $y_1 \gg 1$, we multiply (3.15a) by w_1', and then integrate by parts over $-\infty < y < \infty$ to obtain the solvability condition

$$0 = \int_{-\infty}^{\infty} w_1' LR\, dy \sim -2\int_{-\infty}^{\infty} w_1 w_1' w_2\, dy - \delta^2 \int_{-\infty}^{\infty} w_1^2 w_1' u_1\, dy\,. \tag{3.16}$$

The dominant contribution to the first integral on the right hand-side of (3.16) arises from the region where $y = y_1$. In this region, we use $w(y) \sim 6e^{-y}$ to get $w(y + 2y_1) \sim 6e^{-y-2y_1}$. In this way, we calculate

$$I_1 \equiv 2\int_{-\infty}^{\infty} w_1 w_1' w_2\, dy \sim 2\int_{-\infty}^{\infty} w(y) w'(y) w(y + 2y_1)\, dy \sim 12 e^{-2y_1}\int_{-\infty}^{\infty} e^{-y} w(y) w'(y)\, dy\,. \tag{3.17}$$

Integrating the last expression in (3.17) by parts, and then using $w^2 = w - w''$, we obtain

$$I_1 \sim 6e^{-2y_1}\int_{-\infty}^{\infty} e^{-y}\left(w - w''\right) dy = 6e^{-2y_1} \lim_{y \to -\infty}\left[e^{-y}\left(w + w'\right)\right] = 72 e^{-2y_1}\,. \tag{3.18}$$

To calculate the other integral in (3.16), we integrate by parts and use $u_1(0) = 0$ to get

$$I_2 \equiv \delta^2 \int_{-\infty}^{\infty} w_1^2 w_1' u_1\, dy = -\frac{\delta^2}{3}\int_{-\infty}^{\infty} w_1^3 u_1'\, dy = -\frac{\delta^2}{3}\int_{-\infty}^{\infty} [w(y)]^3\, u_1'(y + y_1)\, dy\,. \tag{3.19}$$

Next, by integrating (3.15b) with $u_1'(0) = 0$, we obtain

$$u_1'(y) \sim \int_0^y [w(s - y_1)]^2 \, ds \,. \tag{3.20}$$

We can then write $u_1'(y + y_1)$ as

$$u_1'(y + y_1) \sim \int_{-y_1}^0 [w(s)]^2 \, ds + \int_0^y [w(s)]^2 \, ds \sim 3 + \int_0^y [w(s)]^2 \, ds \,. \tag{3.21}$$

Here we have used $\int_{-y_1}^0 w^2 \, dy \sim \int_{-\infty}^0 w^2 \, dy = 3$ for $y_1 \gg 1$. The integral on the right hand-side of (3.21) is odd. Therefore, upon substituting (3.21) into (3.19), we get an integral that is readily evaluated as

$$I_2 \sim -\delta^2 \int_{-\infty}^{\infty} [w(y)]^3 \, dy = -\frac{36\delta^2}{5} \,. \tag{3.22}$$

Finally, substituting (3.22) and (3.18) into (3.16), we obtain that y_1 satisfies

$$72 e^{-2y_1} \sim \frac{36\delta^2}{5} \,. \tag{3.23}$$

The product $\gamma \equiv U_0 V_0$ is calculated as $\gamma \sim [w_1(0) + w_2(0)] = 2w(y_1)$. Since $y_1 \gg 1$, we use $w(y) \sim 6e^{-y}$ to get $\gamma \sim 12 e^{-y_1}$, where y_1 satisfies (3.23). Finally, B is determined by $B = \delta \int_0^\infty \left[w_1^2 + w_2^2 \right] dy \sim 6\delta$. This formal construction of a two-bump solution is summarized as follows:

Principal Result 3.2: *Let $\delta = 1/U_0 \ll 1$. Then, along the secondary branch, the core problem (2.10) has a solution where $\gamma \equiv U_0 V_0 \to 0$ from above as $\delta \to 0$. This solution is given asymptotically by*

$$V \sim \delta \left[w(y - y_1) + w(y + y_1) \right] \qquad U \sim \frac{1}{\delta} \left(1 + \delta^2 \left[u_1(y - y_1) + u_1(y + y_1) - 2u(y_1) \right] \right) \,, \tag{3.24a}$$

where $w(y)$ satisfies (A.2), and $u_1(y)$ is given in (3.7). The constants $\gamma \equiv U_0 V_0$, y_1, B, and the local behavior of the $B = B(\gamma)$ curve, are given by

$$B \sim 6\delta \,, \quad \gamma \equiv U_0 V_0 \sim \frac{6\delta\sqrt{2}}{\sqrt{5}} \,, \quad y_1 \sim \ln\left(\sqrt{10}/\delta \right) \,, \quad \delta \ll 1 \,; \quad \gamma \equiv U_0 V_0 \sim \sqrt{2} B/\sqrt{5} \,, \quad B \ll 1 \,. \tag{3.24b}$$

In this limit, we can calculate the limiting form of the norm defined in (2.25). Substituting the inner expansion for v from (3.24a) into (2.25), and using $\delta = B/6$ and $B = A/\coth(l\theta_0)$, we obtain

$$|v|_2 \sim \varepsilon^{-1/2} \sqrt{kD} \left(\int_{-\infty}^{\infty} V^2 \, dy \right)^{1/2} \sim \frac{A\varepsilon^{-1/2}\sqrt{12kD}}{6\coth(\theta_0/k)} \,. \tag{3.25}$$

This analysis shows that on the secondary branch a one-spike equilibrium solution splits into a two-spike solution where the spikes are separated by an amount of order $O(-\ln B)$ as $B \to 0$. This multi-bump analysis is new and is closely related to the pulse-splitting behavior computed below in §6.

The formulae in Principal Results 3.1 and 3.2 are validated in Fig. 2(b), where we plot the asymptotic results (3.13) and (3.25) to the norm $|v|_2$ that are valid at the two extremities of the $B = B(\gamma)$ curve. From this figure, these approximations are decent over most of the curve. In Fig. 5(a) we compare the asymptotic results $\gamma \sim \frac{3}{2} - 11B^2/48$ and $\gamma \sim \sqrt{2}B/\sqrt{5}$ as $B \to 0$, with the numerically computed curve $B = B(\gamma)$. Except near the fold point, these results are rather good. Finally, in Fig. 5(b) we plot the numerically computed U_0 versus γ together with the asymptotic results of Principal Results 3.1 and 3.2.

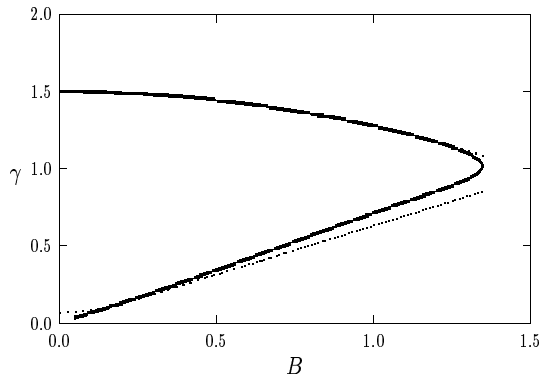

(a) $\gamma = U_0 V_0$ versus B

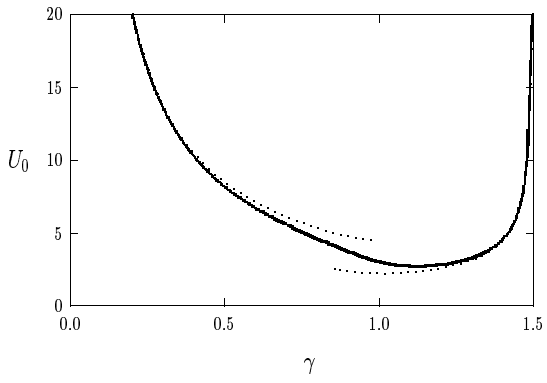

(b) U_0 versus $\gamma = U_0 V_0$

Figure 5: Numerical (solid curves) and asymptotic approximations (dashed curves) obtained from Principal Results 3.1 and 3.2. Left figure: $\gamma = U_0 V_0$ versus B. Right figure: U_0 versus γ.

4 Drift Instabilities: The Small Eigenvalues

Next, we analyze drift instabilities associated with the k-spike equilibrium solution constructed in §2. To do so, we begin by linearizing (1.1) around the equilibrium solution constructed above in Principal Result 2.1. Let v_e and u_e denote this equilibrium solution. We write $v = v_e + e^{\lambda t}\phi$ and $u = u_e + e^{\lambda t}\eta$. Substituting this form into (1.1), we obtain the following eigenvalue problem:

$$\varepsilon^2 \phi_{xx} - \phi + 2A u_e v_e \phi + A\eta v_e^2 = \lambda \phi\,, \qquad D\eta_{xx} - \eta - \eta v_e^2 - 2u_e v_e \phi = \tau\lambda\eta\,, \qquad -1 < x < 1\,. \tag{4.1}$$

Consider the j^{th} inner region for (4.1) where $y = \varepsilon^{-1}(x - x_j)$. Using (2.19a) and (2.19b), we calculate

$$2Au_e v_e \sim 2\left[UV + \frac{\varepsilon A}{\sqrt{D}}\left(UV_1 + U_1 V\right) + \cdots\right], \qquad v_e^2 \sim \frac{D}{\varepsilon^2}\left[V^2 + \frac{2\varepsilon A}{\sqrt{D}} V V_1 + \cdots\right], \tag{4.2}$$

where U, V satisfy (2.10), and U_1, V_1 satisfy (2.16). In this inner region we introduce Φ and N by

$$\phi(x) = \frac{A}{\varepsilon}\Phi\left(y;\varepsilon\right), \qquad \eta(x) = \frac{\varepsilon}{D} N\left(y;\varepsilon\right). \tag{4.3}$$

Substituting (4.3) and (4.2) into (4.1), we obtain the following inner problem on $-\infty < y < \infty$:

$$\Phi_{yy} - \Phi + 2\left[UV + \frac{\varepsilon A}{\sqrt{D}}\left(UV_1 + U_1 V\right) + \cdots\right]\Phi + \left[V^2 + \frac{2\varepsilon A}{\sqrt{D}} V V_1 + \cdots\right] N = \lambda\Phi\,, \tag{4.4a}$$

$$N_{yy} - \left[V^2 + \frac{2\varepsilon A}{\sqrt{D}} V V_1 + \cdots\right] N - 2\left[UV + \frac{\varepsilon A}{\sqrt{D}}\left(UV_1 + U_1 V\right) + \cdots\right]\Phi = \frac{\varepsilon^2}{D}(1 + \tau\lambda) N\,. \tag{4.4b}$$

As suggested by the intermediate regime result (A.13), we look for instabilities associated with small eigenvalues of order $\lambda = O(\varepsilon)$. Therefore, we seek an eigenfunction to (4.4) in the form

$$\Phi(y;\varepsilon) = \Phi_0(y) + \frac{\varepsilon A}{\sqrt{D}}\Phi_1(y) + \cdots, \qquad N(y;\varepsilon) = N_0(y) + \frac{\varepsilon A}{\sqrt{D}}N_1(y) + \cdots, \qquad \lambda = \frac{\varepsilon A}{\sqrt{D}}\lambda_0 + \cdots. \tag{4.5}$$

Substituting (4.5) into (4.4), we find that the leading-order problem is

$$\mathcal{L}\begin{pmatrix} \Phi_0 \\ N_0 \end{pmatrix} \equiv \begin{pmatrix} \Phi_0'' \\ N_0'' \end{pmatrix} + E\begin{pmatrix} \Phi_0 \\ N_0 \end{pmatrix} = 0\,, \qquad E \equiv \begin{pmatrix} -1+2V_0U_0 & V_0^2 \\ -2V_0U_0 & -V_0^2 \end{pmatrix}, \tag{4.6}$$

on $-\infty < y < \infty$. From collecting the $O\left(\varepsilon A/\sqrt{D}\right)$ terms, we obtain

$$\mathcal{L}\Psi = \begin{pmatrix} \lambda_0 & 0 \\ 0 & 0 \end{pmatrix}\begin{pmatrix} \Phi_0 \\ N_0 \end{pmatrix} + \begin{pmatrix} -2(V_0U_1+U_0V_1) & -2V_0V_1 \\ 2(V_0U_1+U_0V_1) & 2V_0V_1 \end{pmatrix}\begin{pmatrix} \Phi_0 \\ N_0 \end{pmatrix}, \qquad \Psi \equiv \begin{pmatrix} \Phi_1 \\ N_1 \end{pmatrix}. \tag{4.7}$$

We look for an odd solution of (4.6) with $\Phi_0 \to 0$ and N_0 bounded as $|y| \to \infty$. For (4.7), the conditions are that $\Phi_1 \to 0$ and N_{1y} is bounded as $|y| \to \infty$. Since $\mathcal{L}$ is not self-adjoint, the calculation of the eigenvalue λ_0 from a solvability condition on (4.7) involves the solution $\Psi^\dagger$ to the homogeneous adjoint problem

$$\mathcal{L}^\dagger\Psi^\dagger \equiv \begin{pmatrix} \Psi_{1yy}^\dagger \\ \Psi_{2yy}^\dagger \end{pmatrix} + E^t\begin{pmatrix} \Psi_1^\dagger \\ \Psi_2^\dagger \end{pmatrix} = 0\,, \tag{4.8}$$

where t denotes transpose. We look for an odd solution to (4.8) where $\Psi_1^\dagger \to 0$ and $\Psi_{2y}^\dagger \to 0$ as $|y| \to \infty$.

By differentiating (2.10), it is clear that a solution to (4.6) is

$$\Phi_0 = c_j V_y\,, \qquad N_0 = c_j U_y\,. \tag{4.9}$$

This solution is odd, and we assume that this is the only solution to (4.6). The constant c_j, associated with this j^{th} inner region, will be determined below after matching to the outer solution. Let $\Psi \equiv (\Phi_1, N_1)^t$. Then, to determine the solvability condition for (4.7), we replace Φ_0 and N_0 in (4.7) by (4.9) and then multiply (4.7) by $\Psi^{\dagger t}$. Upon integrating the resulting expression by parts, we obtain

$$\int_{-\infty}^{\infty} \Psi^{\dagger t}\mathcal{L}\Psi\, dy = \left(\Psi^{\dagger t}\Psi_y - \Psi^t\Psi_y^\dagger\right)|_{-\infty}^{\infty} = c_j\lambda_0 I_2 + c_j I_1\,. \tag{4.10a}$$

Here I_1 and I_2 are defined by

$$I_1 \equiv \int_{-\infty}^{\infty}\left(\Psi_2^{\dagger t} - \Psi_1^{\dagger t}\right)\left[2(UV)_yV_1 + (V^2)_yU_1\right]\, dy\,, \qquad I_2 \equiv \int_{-\infty}^{\infty}\Psi_1^\dagger V_y\, dy\,. \tag{4.10b}$$

Since Ψ and $\Psi^\dagger$ are odd functions and $\Psi_y^\dagger \to 0$ as $y \to \infty$, (4.10a) can be reduced to

$$c_j\lambda_0 I_2 = -c_j I_1 + \Psi_2^\dagger(\infty)\left(N_{1y}(+\infty) + N_{1y}(-\infty)\right)\,. \tag{4.10c}$$

The next step in the analysis is to calculate I_1 explicitly. To do so, we introduce W by $W = (V_{1y}, U_{1y})^t$. Upon differentiating the system (2.16) for V_1 and U_1 with respect to y, it follows that

$$\mathcal{L}W = \begin{pmatrix} -2(UV)_y V_1 - (V^2)_y U_1 \\ 2(UV)_y V_1 + (V^2)_y U_1 \end{pmatrix} . \tag{4.11}$$

Therefore, by using (4.11), I_1 in (4.10b) can be written in terms of W as

$$I_1 = \int_{-\infty}^{\infty} \Psi^{\dagger t} \mathcal{L} W \, dy = \left(\Psi^{\dagger t} W_y - \Psi_y^{\dagger t} W \right) |_{-\infty}^{\infty} + \int_{-\infty}^{\infty} W^t \mathcal{L}^\dagger \Psi^\dagger \, dy \, . \tag{4.12}$$

Using $\mathcal{L}^\dagger \Psi^\dagger = 0$, with $\Psi_1^\dagger \to 0$ and $\Psi_{2y}^\dagger \to 0$ as $|y| \to \infty$, (4.12) reduces to

$$I_1 = 2\Psi_2^\dagger(\infty) U_{1yy}(\infty) = -2\Psi_2^\dagger(\infty) \, . \tag{4.13}$$

Here we used $U_{1yy}(\infty) = -1$ from (2.16b). Finally, substituting (4.13) into (4.10c), we obtain

$$c_j \lambda_0 \int_{-\infty}^{\infty} \Psi_1^\dagger V_y \, dy = 2\Psi_2^\dagger(\infty) \left[\frac{1}{2} \left(N_{1y}(+\infty) + N_{1y}(-\infty) \right) + c_j \right] , \qquad j = 1, \ldots, k \, . \tag{4.14}$$

To determine λ_0 from (4.14) we need to calculate $N_{1y}(\pm\infty)$.

Next, we match this j^{th} inner solution constructed above to the outer solution for (4.1). This will determine $N_{1y}(\pm\infty)$ and the constants c_j, for $j = 1, \ldots, k$. In the outer region, away from $O(\varepsilon)$ regions centered at the spike equilibrium locations, ϕ in (4.1) is exponentially small and η in (4.1) is given by

$$D\eta_{xx} - (1 + \tau\lambda)\eta = \eta v_e^2 + 2u_e v_e \phi \, . \tag{4.15}$$

Since the right hand-side of (4.15) is localized near each $x = x_j$ for $j = 1, \ldots, k$, its effect on the outer solution can be calculated in the sense of distributions. Recalling (4.3), (4.5), and (2.19), we get for x near x_j that the right hand-side of (4.15) is given by

$$\eta v_e^2 + 2u_e v_e \phi \sim \frac{1}{\varepsilon} \left[c_j \left(UV^2 \right)_y + \frac{\varepsilon A}{\sqrt{D}} \left(N_1 V^2 + 2\Phi_1 UV + 2c_j \left(U_y V V_1 + U V_y V_1 + U_1 V V_y \right) \right) \right] . \tag{4.16}$$

Using (4.7) we can write (4.16) as

$$\eta v_e^2 + 2u_e v_e \phi \sim \frac{1}{\varepsilon} \left[c_j \left(UV^2 \right)_y + \frac{\varepsilon A}{\sqrt{D}} N_{1yy} \right] . \tag{4.17}$$

Since UV^2 is even, we obtain in the the sense of distributions that

$$\frac{1}{\varepsilon} \left[c_j \left(UV^2 \right)_y + \frac{\varepsilon A}{\sqrt{D}} N_{1yy} \right] \to 2\varepsilon B c_j \delta'(x - x_j) + \frac{\varepsilon A}{\sqrt{D}} \left(N_{1y}(+\infty) - N_{1y}(-\infty) \right) \delta(x - x_j) \, . \tag{4.18}$$

Here $B \equiv \int_0^\infty UV^2 \, dy$, given in (2.20), is the bifurcation parameter for the core problem (2.10). In this way, the following outer problem for $\eta(x)$ on $|x| \le 1$, with $\eta_x(\pm 1) = 0$, is obtained from (4.15):

$$D\eta_{xx} - (1 + \tau\lambda)\eta = \sum_{i=1}^{k} \left(2\varepsilon B c_i \delta'(x - x_i) + \frac{\varepsilon A}{\sqrt{D}} \left(N_{1y}(+\infty) - N_{1y}(-\infty) \right) \delta(x - x_i) \right) . \tag{4.19}$$

To determine $N_{1y}(\pm\infty)$ in (4.14) we use the matching condition that the far-field behavior of the j^{th} inner solution as $y \to \pm\infty$ must agree with the behavior of $\eta(x)$ as $x \to x_j^{\pm}$. Defining $y = \varepsilon^{-1}(x - x_j)$, we obtain from (4.3) and (4.5) that this matching condition is

$$\frac{\varepsilon}{D}\left(c_j U_y(\pm\infty) + \frac{\varepsilon A}{\sqrt{D}} N_1\right) \sim \eta(x_j^{\pm}) + \varepsilon y \eta_x(x_j^{\pm}) + \cdots . \tag{4.20}$$

Therefore, to match the terms in (4.20), we require that

$$\eta(x_j^{\pm}) = \pm\frac{\varepsilon c_j B}{D}, \qquad N_{1y}(\pm\infty) = \frac{D^{3/2}}{\varepsilon A}\eta_x(x_j^{\pm}) . \tag{4.21}$$

We now solve (4.19) on each subinterval, and we use (4.21) for $\eta(x_j^{\pm})$ and $\eta_x(\pm 1) = 0$. This yields,

$$\eta(x) = \begin{cases} \frac{-\varepsilon B c_1}{D}\frac{\cosh[\theta_\lambda(1+x)]}{\cosh[\theta_\lambda(1+x_1)]}, & -1 < x < x_1 , \\ \frac{\varepsilon B c_j}{D}\frac{\sinh[\theta_\lambda(x-x_{j+1})]}{\sinh[\theta(x_j-x_{j+1})]} - \frac{\varepsilon B c_{j+1}}{D}\frac{\sinh[\theta_\lambda(x-x_j)]}{\sinh[\theta_\lambda(x_{j+1}-x_j)]}, & x_j < x < x_{j+1}, \quad j = 1, \ldots, k-1 , \\ \frac{\varepsilon B c_k}{D}\frac{\cosh[\theta_\lambda(1-x)]}{\cosh[\theta_\lambda(1-x_k)]}, & x_k < x < 1 . \end{cases} \tag{4.22}$$

Here θ_λ is defined by

$$\theta_\lambda \equiv \theta_0\sqrt{1+\tau\lambda}, \qquad \theta_0 \equiv D^{-1/2} . \tag{4.23}$$

Next, we use (4.22) to calculate $N_{1y}(\pm\infty)$ in the matching condition (4.21). Then, we substitute the resulting expressions into (4.14), and we recall the relation $A = B\coth(\theta_0/k)$ from (2.11). In this way, we obtain the following matrix problem for $\boldsymbol{c} = (c_1, \ldots, c_k)^t$ and λ_0:

$$\lambda_0 \boldsymbol{c} = \alpha\left[\frac{\sqrt{1+\tau\lambda}}{2}\tanh\left(\frac{\theta_0}{k}\right)\mathcal{B} - I\right]\boldsymbol{c}, \qquad \mathcal{B} \equiv \begin{pmatrix} d & f & 0 & \cdots & 0 & 0 & 0 \\ f & e & f & \cdots & 0 & 0 & 0 \\ 0 & f & e & \ddots & 0 & 0 & 0 \\ \vdots & \vdots & \ddots & \ddots & \ddots & \vdots & \vdots \\ 0 & 0 & 0 & \ddots & e & f & 0 \\ 0 & 0 & 0 & \cdots & f & e & f \\ 0 & 0 & 0 & \cdots & 0 & f & d \end{pmatrix} . \tag{4.24}$$

The entries of the tridiagonal matrix $\mathcal{B}$ are given by

$$d \equiv \coth\left(\frac{2\theta_\lambda}{k}\right) + \tanh\left(\frac{\theta_\lambda}{k}\right), \qquad e \equiv 2\coth\left(\frac{2\theta_\lambda}{k}\right), \qquad f \equiv \operatorname{csch}\left(\frac{2\theta_\lambda}{k}\right) . \tag{4.25}$$

In (4.24), the parameter α is defined by

$$\alpha \equiv -\frac{\Psi_2^\dagger(\infty)}{\int_0^\infty \Psi_1^\dagger V_y \, dy}, \tag{4.26}$$

Next, we use the following result of Appendix D of [18] for the spectrum of $\mathcal{B}$:

Principal Result 4.1: *The eigenvalues ζ_j and the associated normalized eigenvectors $\boldsymbol{c}_j$ of $\mathcal{B}$ are*

$$\zeta_j = 2\coth\left(\frac{2\theta_\lambda}{k}\right) + 2\operatorname{csch}\left(\frac{2\theta_\lambda}{k}\right)\cos\left(\frac{\pi j}{k}\right), \qquad j = 1, \ldots, k , \tag{4.27a}$$

$$\boldsymbol{c}_k^t = \frac{1}{\sqrt{k}}\left(1, -1, 1, \ldots, (-1)^{k+1}\right); \quad \boldsymbol{c}_{l,j} = \sqrt{\frac{2}{k}}\sin\left(\frac{\pi j}{k}(l - 1/2)\right), \quad j = 1, \ldots, k-1 . \tag{4.27b}$$

Here $\mathbf{c}^t$ *denotes transpose and* $\mathbf{c}_j^t = (c_{1,j}, \ldots, c_{k,j})$.

By substituting (4.27) into (4.24), we obtain k transcendental equations for the eigenvalue λ_0. The eigenvectors in (4.27) determine the constants c_j, for $j = 1, .., k$. In this way, we obtain the following main result for the small eigenvalues:

Principal Result 4.2: *Let* $\varepsilon \ll 1$, *and* $\varepsilon A/\sqrt{D} \ll 1$. *Then, the small eigenvalues* λ *associated with drift instabilities of the k-spike equilibrium solution of Principal Result 2.1 are of order* $O\left(\varepsilon A/\sqrt{D}\right)$, *and satisfy the k transcendental equations,*

$$\lambda \sim \frac{\varepsilon\alpha A}{\sqrt{D}}\left[\sqrt{1+\tau\lambda}\tanh\left(\frac{\theta_0}{k}\right)\left(\coth\left(\frac{2\theta_\lambda}{k}\right)+\operatorname{csch}\left(\frac{2\theta_\lambda}{k}\right)\cos\left(\frac{\pi j}{k}\right)\right)-1\right], \qquad j=1,\ldots,k, \quad (4.28)$$

where α *and* θ_λ *are defined in (4.26) and (4.23). The constant* α *depends on the bifurcation parameter* γ *associated with the core solution of §2. In the inner region near the* j^{th} *spike, the perturbation to the v-component of the equilibrium solution has the following form for some* $\delta \ll 1$*:*

$$v(x,t) \sim \frac{\sqrt{D}}{\varepsilon}\left(V[\varepsilon^{-1}(x-x_j)] + \delta c_j V_y[\varepsilon^{-1}(x-x_j)]e^{\lambda t}\right). \quad (4.29)$$

A central feature of the preceding analysis is that, although the core problem (2.10) must be solved numerically, one can calculate precise formulae for the small eigenvalues in terms of a single numerically-determined constant, α, that is related to the core problem. For $k = 1$, (4.28) reduces to

$$\lambda \sim \frac{\varepsilon\alpha A}{\sqrt{D}}\left[\sqrt{1+\tau\lambda}\tanh(\theta_0)\tanh(\theta_\lambda)-1\right]. \quad (4.30)$$

This one-spike result is very similar in form to the result (A.8b) of Principal Result A.3 in the intermediate parameter regime. The only difference between (4.30) and (A.8b) is in a multiplicative factor. We now show that these two formulae do in fact agree if we let $A \to 0$ in (4.30).

To show this, we must calculate the limiting behavior of α in (4.26) along the primary branch as $B \to 0$ and $\gamma \to 3/2$. In this limit, we recall from Principal Result 3.1 that $V \sim \delta w$, and $U \sim \delta^{-1}$, where $\delta \sim A/[3\coth(\theta_0)]$. Here w is the spike profile given in (A.2). Therefore, for $\delta \ll 1$, the homogeneous adjoint problem (4.8) reduces to

$$\psi_{1yy}^\dagger + (-1+2w)\psi_1^\dagger - 2w\psi_2^\dagger \sim 0, \qquad \psi_{2yy}^\dagger + \delta^2 w^2\left(\psi_1^\dagger - \psi_2^\dagger\right) \sim 0. \quad (4.31)$$

The solution to this limiting system is odd and is given, up to a normalization constant, by

$$\psi_1^\dagger = w_y + O(\delta^2), \qquad \psi_2^\dagger = -\frac{\delta^2}{3}\int_0^y [w(s)]^3\,ds + O(\delta^4). \quad (4.32)$$

Therefore, for $\delta \ll 1$, we have

$$\alpha \equiv -\frac{\Psi_2^\dagger(\infty)}{\int_0^\infty \Psi_1^\dagger V_y\,dy} \sim \frac{\delta}{3}\left(\frac{\int_0^\infty w^3\,dy}{\int_0^\infty w_y^2\,dy}\right). \quad (4.33)$$

To calculate the integral in (4.33) we use $w(y) = \frac{3}{2}\operatorname{sech}^2(y/2)$. This yields $\alpha = 2\delta$. Then, using $\delta \sim A/[3\coth(\theta_0)]$, and $B = A\tanh\theta_0$, we obtain the limiting result

$$\alpha \sim \frac{2A}{3}\tanh\theta_0 \sim \frac{2B}{3}, \qquad \text{for} \quad A \ll 1. \quad (4.34)$$

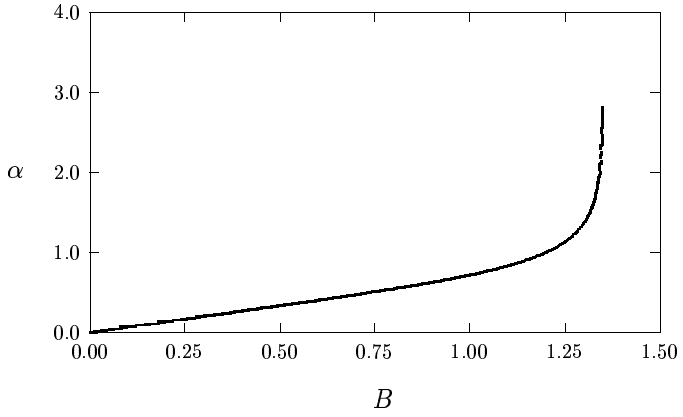

Figure 6: Plot of α, defined in (4.26), versus B along the primary solution branch of the B, γ parameter plane. The right endpoint of this curve corresponds to the fold point $B = 1.347$.

By substituting (4.34) into (4.30) we do indeed recover (A.8b) of Appendix A.

To determine α in (4.26) we compute the numerical solution to the adjoint problem (4.8), and then evaluate the integral in (4.26) with a numerical quadrature. In Fig. 6 we plot α versus B along the primary branch in the B, γ parameter plane of Fig. 2(a). Although we are not able to give a rigorous proof of the sign of α, our computations show that $\alpha > 0$ along this branch.

Since $\lambda = O(\varepsilon)$, then $\lambda\tau \ll 1$ for $\tau \ll O(\varepsilon^{-1})$. For $\tau \ll O(\varepsilon^{-1})$, (4.28) reduces to

$$\lambda \sim -\frac{\varepsilon\alpha A}{\sqrt{D}}\mathrm{sech}^2\left(\frac{\theta_0}{k}\right)\left[1 - \frac{1}{2}\left(1 + \cos\left(\pi j/k\right)\right)\right], \qquad j = 1, \ldots, k\,. \tag{4.35}$$

Since $\alpha > 0$, we conclude that $\lambda < 0$ for $j = 1, \ldots, k$. This leads to the following stability result:

Principal Result 4.3: *Let $\varepsilon \ll 1$, $\tau \ll O(\varepsilon^{-1})$, and $\varepsilon A/\sqrt{D} \ll 1$. Then, along the primary branch of the B, γ parameter plane, the k-spike equilibrium solution of Principal Result 2.1 is stable with respect to drift instabilities associated with the small eigenvalues.*

We now determine instabilities associated with (4.28) when $\lambda = O(\varepsilon^{-1})$. To analyze (4.28) it is convenient to introduce the new variables τ_d, ω, and ξ, defined by

$$\lambda = \left(\frac{\varepsilon\alpha A}{\sqrt{D}}\right)\omega\,, \qquad \tau = \left(\frac{\sqrt{D}}{\varepsilon\alpha A}\right)\tau_d\,, \qquad \xi = \tau_d\omega\,. \tag{4.36}$$

Substituting (4.36) into (4.28), we obtain that ξ satisfies $F_j(\xi) = 0$, where

$$F_j(\xi) \equiv \frac{\xi}{\tau_d} - G_j(\xi)\,, \tag{4.37a}$$

$$G_j(\xi) \equiv \sqrt{1+\xi}\tanh\left(\frac{\theta_0}{k}\right)\left(\coth\left(\frac{2\theta_0\sqrt{1+\xi}}{k}\right) + \mathrm{csch}\left(\frac{2\theta_0\sqrt{1+\xi}}{k}\right)\cos\left(\frac{\pi j}{k}\right)\right) - 1\,, \quad j = 1, \ldots, k\,. \tag{4.37b}$$

In terms of the roots $F(\xi) = 0$, the scaled eigenvalues ω are given by $\omega = \xi/\tau_d$.

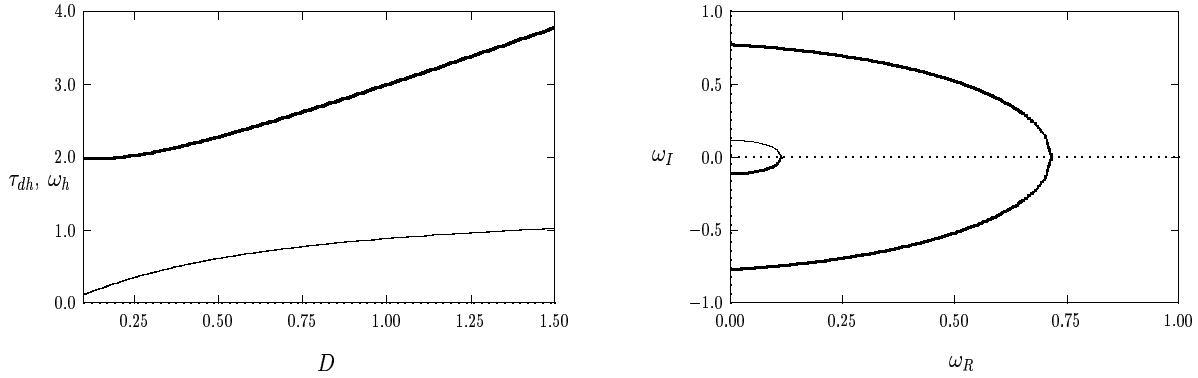

(a) τ_{dh} and ω_h

(b) eigenvalues in right half-plane

Figure 7: A one-spike solution. Left figure: The Hopf bifurcation value τ_{dh} (heavy solid curve) and the frequency ω_h (solid curve) versus D. Right figure: The eigenvalues $\omega = \omega_R + i\omega_I$ in the right half-plane for $\tau_{dh} \le \tau \le \tau_{dm}$ when $D = 0.75$ (heavy solid curve) and $D = 0.1$ (solid curve).

For the one-spike case $k = 1$, (4.37) reduces to the problem (A.10) of Appendix A for the small eigenvalue of a one-spike solution in the intermediate regime. Therefore, Principal Result A.4 of Appendix A, established in [21], also applies to the stability of a one-spike solution in the pulse-splitting regime.

Principal Result 4.4: *Let $\varepsilon \ll 1$, $\tau = O(\varepsilon^{-1})$, $k = 1$, and $\varepsilon A/\sqrt{D} \ll 1$. Then, there exists a unique value τ_{dh}, depending on D, for which there is a complex conjugate pair of pure imaginary eigenvalues when $\tau_d = \tau_{dh}$. For any $\tau_d > \tau_{dh}$ there are exactly two eigenvalues in the right half-plane. These eigenvalues merge onto the positive real axis when $\tau_d = \tau_{dm}$, and they remain there for all $\tau_d > \tau_{dm}$. In terms of τ, the Hopf bifurcation in the spike location occurs when $\tau = \tau_{TW}$, where*

$$\tau_{TW} \sim \left(\frac{\sqrt{D}}{\varepsilon\alpha A}\right)\tau_d\,. \tag{4.38}$$

To determine τ_{dh} for a one-spike solution where $k = 1$ we numerically determine the zeroes of $F_1(\xi) = 0$ on the imaginary axis. The zeroes occur when $\xi = i\xi_h$ and $\tau_d = \tau_{dh}$, which yields $\omega_h \equiv \xi_h/\tau_{dh}$. In Fig. 7(a) we plot τ_{dh} and ω_h versus D. To illustrate Principal Result 4.4, we compute the roots of $F_1(\xi) = 0$ with $\xi = \xi_R + i\xi_I$ on the range $\tau_{dh} \le \tau_d \le \tau_{dm}$. In terms of $\omega = \xi/\tau_d \equiv \omega_R + i\omega_I$, in Fig. 7(b) we plot this path in the complex plane for $D = 0.75$ and $D = 0.1$.

We now consider the multi-spike case where $k > 1$. We first look for roots of $F_j(\xi) = 0$ on the positive imaginary axis $\xi = i\xi_I$ with $\xi_I \ge 0$. By separating (4.37) into real and imaginary parts, we obtain

$$F_{jR}(\xi_I) = -G_{jR}(\xi_I)\,, \qquad F_{jI}(\xi_I) = \frac{\xi_I}{\tau_d} - G_{jI}(\xi_I)\,, \qquad j = 1,\ldots,k\,, \tag{4.39}$$

where $F_{jR}(\xi_I) = \mathrm{Re}(F_j(i\xi_I))$, $F_{jI}(\xi_I) = \mathrm{Im}(F_j(i\xi_I))$, $G_{jR}(\xi_I) = \mathrm{Re}(G_j(i\xi_I))$, $G_{jI}(\xi_I) = \mathrm{Re}(G_j(i\xi_I))$.

Using (4.37), it is readily seen that $G_{jR}(0) < 0$ and that $G_{jR}(\xi_I)$ is monotonically increasing with $G_{jR}(\xi_I) \to +\infty$ as $\xi_I \to \infty$. Therefore, $F_{jR}(\xi_I) = 0$ has a unique root, which we label by ξ_{Ij}. Then, setting $F_{jI}(\xi_{Ij}) = 0$, we obtain the critical value τ_{dj}, defined by

$$\tau_{dj} \equiv \frac{\xi_{Ij}}{G_{jI}(\xi_{Ij})}\,, \qquad j = 1, \ldots, k\,. \tag{4.40}$$

In terms of τ_{dj}, we define $\omega_j \equiv \xi_{Ij}/\tau_{dj}$. For each j, τ_{dj} denotes the unique value of τ_d where there is a complex conjugate pair of small eigenvalues on the imaginary axis.

By adapting the proof of Proposition 5.2 of [21], we can prove that, for each fixed $j = 1, \ldots, k$, there are exactly two roots of $F_j(\xi) = 0$ for any $\tau_d > \tau_{dj}$. In addition, these roots merge onto the positive real axis when $\tau_d = \tau_{dj}^* > \tau_{dj}$, and they remain there for $\tau_d > \tau_{dj}^*$. To show this, we first derive a formula for the number M_j of zeroes of $F_j(\xi) = 0$ in the right half-plane. To do so, we calculate the winding number of $F_j(\xi)$ over the counterclockwise contour composed of the imaginary axis $-iR \le \mathrm{Im}(\xi) \le iR$ and the semi-circle Γ_R, given by $|\xi| = R > 0$, for $\mathrm{Re}(\xi) > 0$. For any $\tau_d > 0$, it is easy to see from (4.37) that the change in the argument of $F_j(\xi)$ over Γ_R as $R \to \infty$ is π. Since $F_j(\xi)$ is analytic in $\mathrm{Re}(\xi) \ge 0$, and $F_j(\overline{\xi}) = \overline{F_j(\xi)}$, the argument principle yields that

$$M_j = \frac{1}{2} + \frac{1}{\pi}\left[\arg F_j\right]_{\Gamma_I}\,. \tag{4.41}$$

Here $[\arg F_j]_{\Gamma_I}$ denotes the change in the argument of $F_j(\xi)$ along the semi-infinite imaginary axis $\Gamma_I = i\xi_I$, $0 \le \xi_I < \infty$, traversed in the downwards direction.

To calculate M_j, we note that $F_{jI} = O(\xi_I)$ and $F_{jR} = O(\sqrt{\xi_I})$ as $\xi_I \to \infty$, and that $F_{jI}(0) = 0$ with $F_{jR}(0) > 0$. This implies that $\arg F_j = \pi/2$ as $\xi_I \to +\infty$, and $\arg F_j = 0$ at $\xi_I = 0$. Since the root to $F_{jR}(\xi_I) = 0$ is unique and independent of τ_d, the change in the argument $[\arg F_j]_{\Gamma_I}$ is determined by the sign of $F_{jI}(\xi_I)$ at the unique root of $F_{jR}(\xi_I) = 0$. In this way, we get that $[\arg F_j]_{\Gamma_I}$ is $3\pi/2$ when $\tau > \tau_{dj}$ and is $-\pi/2$ when $0 < \tau_d < \tau_{dj}$. From (4.41) this yields that $M_j = 2$ when $\tau_d > \tau_{dj}$ and $M_j = 0$ when $0 < \tau_d < \tau_{dj}$. Therefore, the roots of $F_j(\xi) = 0$ have a strict transversal crossing into the right half-plane as τ is increased past τ_{dj}. The fact that that the roots of $F_j(\xi) = 0$ merge onto the real axis at some value τ_{dj}^* follows from the simple observation that $G_j(\xi)$ in (4.37b) is an increasing, and concave, function when $\xi > 0$ is real, and that $G_j(0) < 0$. This proves that when ξ is real, $F_j(\xi) = 0$ will have exactly two roots for $\tau \ge \tau_{dj}^*$, where τ_{dj}^* is determined from the condition that ξ/τ_d intersects $G_j(\xi)$ tangentially at a unique point when $\tau = \tau_{dj}^*$. This leads to the following stability result for a k-spike solution:

Principal Result 4.5: *Let $\varepsilon \ll 1$, $\tau = O(\varepsilon^{-1})$, and $\varepsilon A/\sqrt{D} \ll 1$. Then, along the primary branch of the B, γ parameter plane, the k-spike equilibrium solution of Principal Result 2.1 is stable when $0 < \tau < \tau_{TW}$, and is unstable when $\tau > \tau_{TW}$. The stability of this solution is lost due to a Hopf bifurcation in the spike locations that occurs when $\tau = \tau_{TW}$, where*

$$\tau_{TW} \sim \left(\frac{\sqrt{D}}{\varepsilon\alpha A}\right)\tau_{dh}\,, \qquad \tau_{dh} \equiv \min_{j=1,\ldots,k}(\tau_{dj})\,. \tag{4.42}$$

For a two-spike solution where $k = 2$, in Fig. 8(a) we plot the numerically computed functions τ_{dj} for $j = 1, 2$ versus D. A similar plot for the three-spike case is shown in Fig. 8(b). These numerical results,

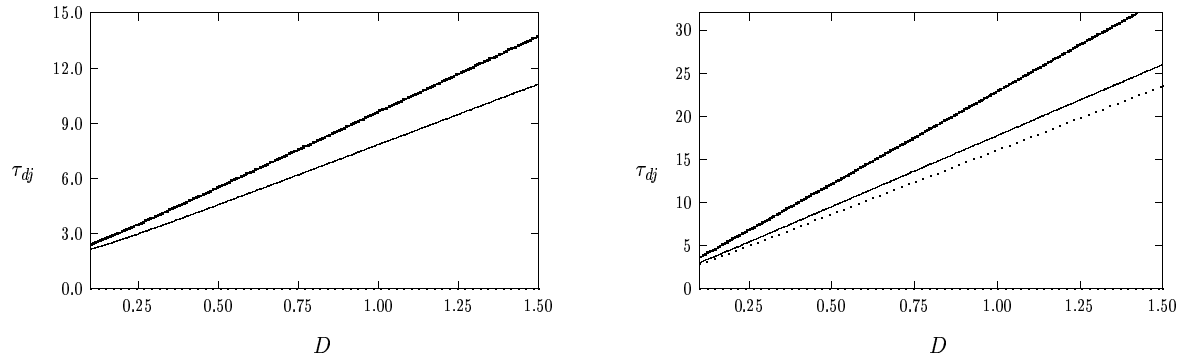

(a) Two spikes: τ_{dj} for $j = 1, 2$

(b) Three spikes: τ_{dj} for $j = 1, 2, 3$

Figure 8: The values τ_{dj} for $j = 1, \ldots, k$ versus D where complex conjugate eigenvalues enter the right half-plane. The Hopf bifurcation value τ_{dh} is the minimum of these values. Left figure: a two-spike solution, with $j = 1$ (heavy solid curve) and $j = 2$ (solid curve). Right figure: a three-spike solution with $j = 1$ (heavy solid curve), $j = 2$ (solid curve), and $j = 3$ (dashed curve).

together with other results (not shown) for larger ranges of D and for $k > 3$, suggest that in each case τ_{dh} is determined by the $j = k$ mode. From (4.27b), we see that the effect of the $j = k$ mode on the small-scale oscillatory behavior of the spike locations is to introduce a breathing-type instability whereby consecutive spike-layer locations are 180° degrees out of phase. This leads to the following conjecture:

Conjecture 4.6: *Let $\varepsilon \ll 1$, and $\varepsilon A/\sqrt{D} \ll 1$. Then, along the primary branch, a k-spike solution first loses its stability to a breathing-type instability at the value $\tau = \tau_{TW} \sim \left(\frac{\sqrt{D}}{\varepsilon\alpha A}\right)\tau_{dk}$. In terms of the v-component, this small-scale oscillatory instability takes the form,*

$$v(x,t) \sim \frac{\sqrt{D}}{\varepsilon}\sum_{j=1}^{k} V\left(\varepsilon^{-1}[x - x_j(t)]\right), \qquad x_j(t) \sim x_j(0) + \delta c_j \cos\left(\frac{\varepsilon\alpha A\omega_k t}{\sqrt{D}} - \phi\right), \tag{4.43}$$

where $\delta \ll 1$, and ϕ is arbitrary. Here $c_j = (-1)^j$ and $x_j(0) = -1 + (2j-1)/k$ for $j = 1, \ldots, k$. In addition, $\omega_k = \xi_{Ik}/\tau_{dk}$, where $F_k(i\xi_{Ik}) = 0$.

5 Stability of the Profile: The Large Eigenvalues

We now determine the stability of the k-spike equilibrium solution of Principal Result 2.1 with respect to eigenvalues λ with $\lambda = O(1)$ as $\varepsilon \to 0$. In the high feed-rate regime, the NLEP eigenvalue analysis of [7] and [20] does not apply due to a strong coupling of the inner solution, as evidenced by the core problem. Therefore, a different approach is required. Assuming that $\tau \ll O(\varepsilon^{-2})$, we can repeat the calculation leading to (4.4) to derive the following leading-order eigenvalue problem in the j^{th} inner region:

$$\Phi_{0yy} - \Phi_0 + 2UV\Phi_0 + V^2 N_0 = \lambda\Phi_0\,, \qquad N_{0yy} - V^2 N_0 - 2UV\Phi_0 = 0\,, \qquad -\infty < y < \infty\,. \tag{5.1}$$

We seek an even eigenfunction of (5.1) for which $\Phi_0 \to 0$. Upon matching to the outer region below, the other boundary condition is that $N_{0y} \to 0$ as $|y| \to \infty$.

To derive such an asymptotic boundary condition for N_0, we consider the outer solution for η given in (4.15). Since Φ_0 and N_0 are even, we obtain in place of (4.16) that near x_j,

$$\eta v_e^2 + 2u_e v_e \phi \sim \frac{1}{\varepsilon}\left(2UV\Phi_0 + V^2 N_0\right) \sim \frac{1}{\varepsilon} N_{0yy}\,. \tag{5.2}$$

Therefore, since N_{0y} is odd, we get in place of (4.19) that

$$D\eta_{xx} - (1+\tau\lambda)\eta = 2\sum_{i=1}^{k} N_{0y}(\infty)\delta(x-x_i)\,, \quad -1 < x < 1\,; \qquad \eta_x(\pm 1) = 0\,. \tag{5.3}$$

The solution to (5.3) can be written as

$$\eta(x) = -2\sum_{i=1}^{k} N_{0y}(\infty) G(x;x_i)\,, \tag{5.4}$$

where $G(x;x_i)$ is the Green's function satisfying (A.3) of Appendix A. The leading-order matching condition analogous to (4.20) is that $\varepsilon D^{-1} N_0$ as $|y| \to \infty$ agrees with $\eta(x)$ as $x \to x_j$. This enforces that $N_{0y}(\infty) = 0$. Therefore, (5.1) with $N_{0y}(\infty) = 0$ holds for each eigenvalue problem.

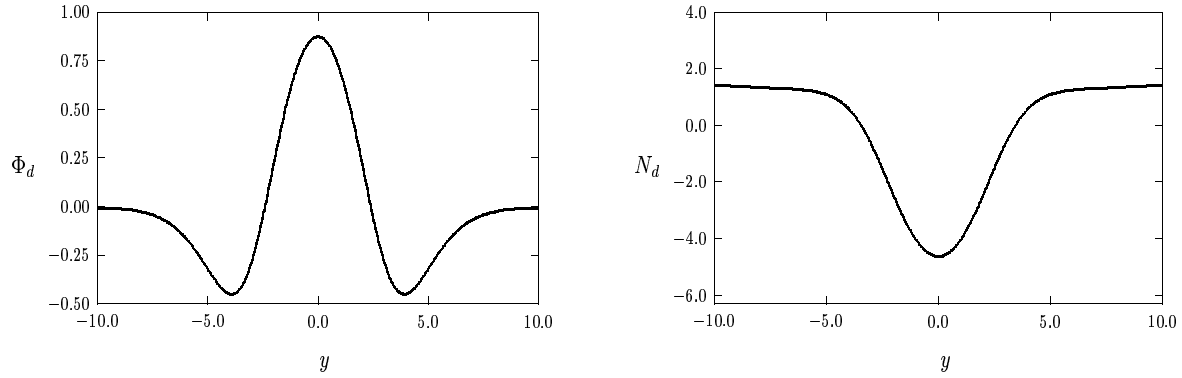

(a) $\Phi_d(y)$ (b) $N_d(y)$

Figure 9: The dimple eigenfunction $\Phi_d = V_\gamma(y)$ (left figure) and $N_d = U_\gamma(y)$ (right figure) at $\gamma = \gamma_c \approx 1.02$.

We now consider the spectrum of (5.1). Recall from the core problem (2.10) that at the fold point $\gamma = \gamma_c$ of the $B = B(\gamma)$ curve, we have that $B'(\gamma_c) = 0$. This implies that (5.1) has an eigenfunction with zero eigenvalue at this point. To see this, we differentiate (2.10) and (2.12) with respect to γ to get

$$V_\gamma'' - V_\gamma + 2UVV_\gamma + V^2 U_\gamma = 0\,, \qquad U_\gamma'' = U_\gamma V^2 + 2UVV_\gamma\,, \qquad -\infty < y < \infty\,, \tag{5.5a}$$

$$V_\gamma \to 0\,, \qquad U_\gamma \sim B'(\gamma)|y| + \chi'(\gamma)\,, \qquad \text{as} \quad y \to \pm\infty\,. \tag{5.5b}$$

Therefore, at the fold point where $\gamma = \gamma_c$ and $B'(\gamma_c) = 0$, we compare (5.1) and (5.5) to conclude that

$$\Phi_0(y) = \Phi_d(y) \equiv V_\gamma\,, \qquad N_0(y) = N_d(y) \equiv U_\gamma\,, \quad \text{when} \quad \gamma = \gamma_c\,, \tag{5.6}$$

is an eigenfunction of (5.1) with $\lambda = 0$. This eigenfunction Φ_d, which is computed numerically, is shown is shown in Fig. 9 to have a dimple shape. This dimple property was also observed in [30].

An analytical study of the spectrum of (5.1) as a function of γ does not appear to be possible. Hence, we will compute the spectrum numerically. We discretize (5.1) on the interval $[0, L]$ using centered differences, ensuring that Φ_0 and N_0 are even functions and that $N_{0y} \to 0$ at $y = L$. We label $y_1 = 0$, $y_m = L$, with $m > 1$, and we choose a meshsize $h = L/(m-1)$. This leads to the discrete formulation

$$(\mathcal{M} - I + \Lambda_2)\,\boldsymbol{\Phi_0} + \Lambda_1 \boldsymbol{N_0} = \lambda \boldsymbol{\Phi_0}\,, \qquad (\mathcal{M} - \Lambda_1)\,\boldsymbol{N_0} = \Lambda_2 \boldsymbol{\Phi_0}\,, \tag{5.7a}$$

so that

$$\left(\mathcal{M} - I + \Lambda_2 + \Lambda_1\,(\mathcal{M} - \Lambda_1)^{-1}\,\Lambda_2\right)\boldsymbol{\Phi_0} = \lambda \boldsymbol{\Phi_0}\,, \tag{5.7b}$$

where $\boldsymbol{\Phi_0} = (\Phi_0(y_1), \ldots, \Phi_0(y_m))^t$, $\boldsymbol{N_0} = (N_0(y_1), \ldots, N_0(y_m))^t$. In addition, Λ_1 and Λ_2 are $m \times m$ diagonal matrices, and $\mathcal{M}$ is a tridiagonal matrix of the same size. More specifically, we have

$$\Lambda_{1\,ii} = V^2(y_i)\,, \qquad \Lambda_{2\,ii} = 2U(y_i)V(y_i)\,, \qquad \mathcal{M} \equiv \frac{1}{h^2}\begin{pmatrix} -2 & 2 & 0 & \cdots & 0 & 0 & 0 \\ 1 & -2 & 1 & \ddots & \ddots & 0 & 0 \\ 0 & \ddots & \ddots & \ddots & \ddots & \ddots & 0 \\ \vdots & \ddots & \ddots & \ddots & \ddots & \ddots & \vdots \\ 0 & \ddots & \ddots & \ddots & \ddots & \ddots & 0 \\ 0 & 0 & \ddots & \ddots & 1 & -2 & 1 \\ 0 & 0 & 0 & \cdots & 0 & 2 & -2 \end{pmatrix}. \tag{5.7c}$$

The eigenvalues of the discrete problem (5.7b) were computed using LAPACK [1] on a domain with $L = 12$ and $m = 200$. Increasing the number of meshpoints and the domain length did not change the results noticeably. In Fig. 10(a) and Fig. 10(b) we plot the real and imaginary parts of the eigenvalues as a function of γ. The plot in Fig. 10(a) shows that the primary solution branch of Fig. 2(a) corresponding to $1.02 < \gamma < 1.5$ is stable with respect to the large eigenvalues, while the secondary branch corresponding to $0 < \gamma < 1.02$ is unstable due to positive real eigenvalue.

For D small, we have shown in Principal Result 2.2 that there is an approximate lining-up property of k-spike equilibrium branches associated with the core solution. Moreover, the numerical computations above have shown that there is a dimple-shaped eigenfunction at the saddle-node bifurcation point A_{pk}. In addition, we have shown numerically that the primary solution branch is stable with respect to the large eigenvalues when $\tau \ll O(\varepsilon^{-2})$, but that the secondary branch is always unstable. In §4 we showed that the primary solution branch is stable with respect to drift instabilities when $\tau \ll O(\varepsilon^{-1})$. Therefore, the pulse-splitting criteria of [10] are satisfied when $\tau \ll O(\varepsilon^{-1})$. This leads us to the following conjecture concerning the number of pulse-splitting events and the final equilibrium state under (1.1):

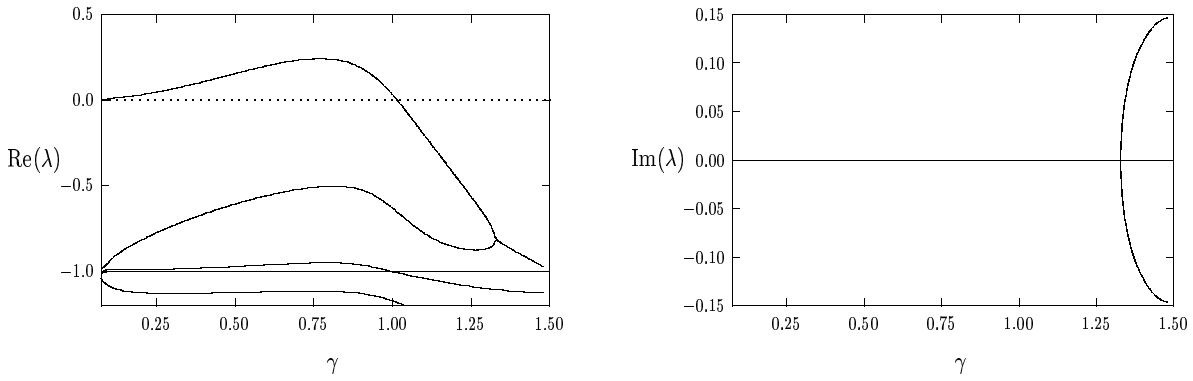

(a) Re(λ) versus γ

(b) Im(λ) versus γ

Figure 10: Left figure: Re(λ) versus γ for the spectrum of (5.1). There is an eigenvalue with a positive real part only when $0 < \gamma < 1.02$. Right figure: Im(λ) versus γ for the spectrum of (5.1).

Conjecture 5.1: *Let $\varepsilon \ll 1$, $\tau \ll O(\varepsilon^{-1})$, and $\varepsilon A/\sqrt{D} \ll 1$. Suppose that we have even one-spike initial data centered at the origin. Then, the final equilibrium state is stable with respect to both the large and small eigenvalues, and it has 2^m spikes where, for some integer $m \geq 0$, A satisfies*

$$A_{p2^{m-1}} < A < A_{p2^m} \,. \tag{5.8}$$

Here A_{pk} is the existence threshold, which depends on D, defined in (2.26).

Finally, we determine whether the primary solution branch can become unstable with respect to a Hopf bifurcation of the large eigenvalues when $\tau = O(\varepsilon^{-2})$. For this range of τ, the slow drift instabilities of §5 are also present. In (4.4) we let $\tau = O(\varepsilon^{-2})$. In place of (5.1), we get the eigenvalue problem

$$\Phi_{0yy} - \Phi_0 + 2UV\Phi_0 + V^2 N_0 = \lambda\Phi_0\,; \qquad N_{0yy} - V^2 N_0 - 2UV\Phi_0 = \lambda\tau_L N_0\,, \qquad -\infty < y < \infty\,, \tag{5.9a}$$

where $\tau_L = O(1)$ is related to τ by

$$\tau = \frac{D\tau_L}{\varepsilon^2}\,. \tag{5.9b}$$

In place of (5.7), the eigenvalues of (5.9) are approximated by the eigenvalues of

$$\begin{pmatrix} \mathcal{M} - I + \Lambda_2 & \Lambda_1 \\ -\Lambda_2 & \mathcal{M} - \Lambda_1 \end{pmatrix} \begin{pmatrix} \boldsymbol{\Phi_0} \\ \boldsymbol{N_0} \end{pmatrix} = \lambda \begin{pmatrix} I & 0 \\ 0 & \tau_L I \end{pmatrix} \begin{pmatrix} \boldsymbol{\Phi_0} \\ \boldsymbol{N_0} \end{pmatrix}. \tag{5.10}$$

For each τ_L, we compute the eigenvalues of this block matrix problem using a generalized eigenvalue problem solver from LAPACK [1]. Newton's method is then used to determine the value τ_{Lh} of τ_L where eigenvalues first enter the right half-plane. The computations show that these eigenvalues enter the right half-plane through a Hopf bifurcation. In Fig. 11(a) and Fig. 11(b) we plot the Hopf bifurcation value τ_{Lh} and the corresponding $\mathrm{Im}(\lambda) = \lambda_{Ih}$ for each point along the primary solution branch.

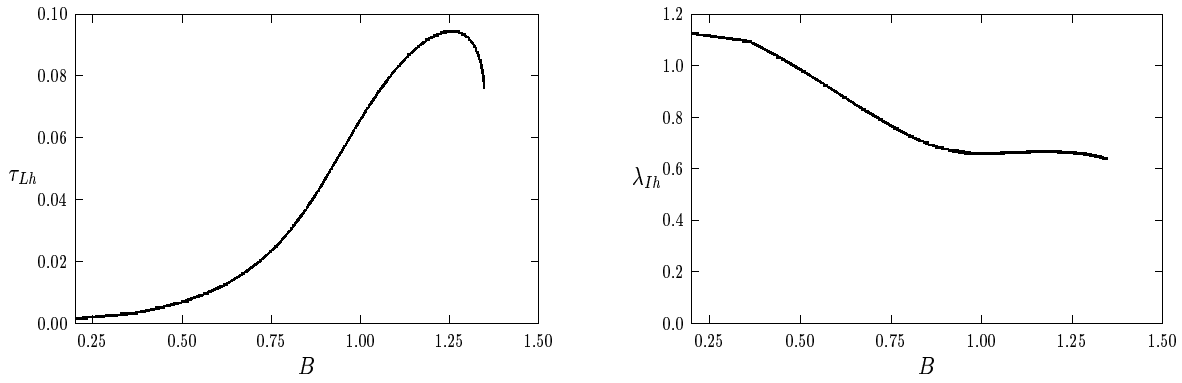

(a) τ_{Lh} versus B

(b) λ_{Ih} versus B

Figure 11: Left figure: There is a Hopf bifurcation in the spike amplitude when $\tau = D\tau_{Lh}/\varepsilon^2$. Right figure: the value $\lambda = i\lambda_{Ih}$ where there is a pair of complex conjugate eigenvalues on the imaginary axis.

6 Numerical Experiments

In this section we perform some numerical experiments on (1.1) in the pulse-splitting regime to test Conjectures 4.6 and 5.1, and to observe instabilities when τ is asymptotically large. The results below are computed using the routine D03PCF of the NAG library [31] with 1500 uniformly spaced meshpoints. The initial condition for (1.1) is taken to be

$$v(x,0) = \frac{\sqrt{D}}{\varepsilon} V(0) \sum_{j=1}^{k} \operatorname{sech}^2\left(\frac{\varepsilon^{-1}(x-x_j)}{2}\right), \qquad u(x) = 1 - \left(1 - \frac{\varepsilon}{A\sqrt{D}} U(0)\right) \sum_{j=1}^{k} G(x;x_j)/a_g\,. \quad (6.1)$$

Here a_g is defined in (A.1c). In addition, $U(0)$, $V(0)$ denote the solution to the core problem (2.10) at $y = 0$ and at the fold point where $\gamma = \gamma_c$.

Experiments 1-3: (Pulse-Splitting; No Instabilities) For each of these examples $\tau \ll O(\varepsilon^{-1})$, and so there are no drift or large eigenvalue instabilities. Consider a one-spike initial condition for (1.1) with $\varepsilon = 0.02$, $D = 0.75$, $A = 2.0$, and $\tau = 2.0$. For these values, $\varepsilon A/\sqrt{D} = 0.046 \ll 1$, and from (2.26) we get $A_{p1} = 1.644$, $A_{p2} = 2.587$, and $A_{p4} = 4.795$. Since $A_{p1} < A < A_{p2}$, there is no one-spike equilibrium solution and we predict only one pulse-splitting event. The final state should be a two-spike solution. In Fig. 12(a) we plot v at three different times. In Fig. 12(b) we plot the locations x_j of the maxima of v as a function of time. Indeed, there is only one pulse-splitting event at $t \approx 6.0$. In Experiment 2 we keep the same parameter values, but increase A to $A = 3.0$, so that $\varepsilon A/\sqrt{D} = 0.069 \ll 1$. In this case, since $A_{p2} < A < A_{p4}$, we now expect two pulse-splitting events and a four-spike final equilibrium state. In Fig. 12(c) we plot v at three different times, and in the t versus x_j plot of Fig. 12(d) we show two pulse-splitting events at $t \approx 2.0$ and $t \approx 60.0$.

Next, in Experiment 3, we consider a three-spike initial condition for (1.1) with $\varepsilon = 0.01$, $D = 0.1$,

$A = 1.9$, and $\tau = 2.0$. For these values $\varepsilon A/\sqrt{D} = 0.06$. From (2.26) we get $A_{p3} = 1.719$, and $A_{p6} = 2.788$. Since $A_{p3} < A < A_{p6}$, we predict one pulse-splitting event (which occurs at $t = 19.5$), and a six-spike final equilibrium state. This is indeed what is observed in Fig. 12(e) and Fig. 12(f).

In terms of a different dimensionless formulation of the GS model other than (1.1) and, for certain parameter values, an eight-spike final equilibrium state was computed in [3] and [39]. Those parameter values correspond to $\varepsilon = 0.0119$, $D = 0.0555$, $A = 1.7901$, $\tau = 1.339 = O(1)$, $A_{p4} = 1.7135$, and $A_{p8} = 2.7725$. Since $A_{p4} < A < A_{p8}$, and τ is below the drift instability threshold, Conjecture 5.1 correctly predicts the eight-spike final equilibrium.

Experiment 4: (Asymmetric Initial Data) Next, we consider one-spike initial data not centered at the origin, but instead at $x_0(0) = 0.35$. We also choose $\varepsilon = 0.02$, $D = 0.75$, and $\tau = 2.0$. For these values, (2.26) yields $A_{p1} = 1.644$, $A_{p2} = 2.587$, $A_{p3} = 3.6707$, and $A_{p4} = 4.7950$. For $A = 3.0$, in Fig. 13(a) we plot t versus the spike locations x_j, showing one splitting event and a three-spike final equilibrium state. Alternatively, for $A = 4.0$, in Fig. 13(b) we show a four-spike final equilibrium state. For the first value of A, where $A_{p2} < A < A_{p3}$, our theory predicts either a three or a four-spike final equilibrium state. A detailed analysis of the dynamics of these patterns is needed to determine the final equilibrium state.

In the next five experiments, we examine drift and large eigenvalue instabilities that occur when τ is asymptotically large.

Experiment 5: (Drift and Profile Instability, One Spike) We take a one-spike solution as initial data, centered at $x_0(0) = 0.05$, with $D = 0.25$, $A = 1.35$, $\varepsilon = 0.01$, and $k = 1$. For these values, we calculate $B = 1.301$ and $\alpha = 1.366$ from Fig. 6. From Fig. 11(a) and (5.9b), we get that the Hopf bifurcation threshold of the spike profile is $\tau_H = 230$. From (4.38), the oscillatory drift instability threshold is $\tau_{TW} = 55$. In Fig. 14(a) we show an oscillatory instability in the spike location. In Fig. 14(b) we show an oscillatory instability of the spike amplitude for a spike that is initially centered at the origin.

Experiment 6: (Drift and Profile Instability, Two Spikes) Next, we consider instabilities of a two-spike solution when $D = 0.1$, $A = 1.4$, $\varepsilon = 0.01$, and $k = 2$. For these values, we calculate $B = 1.286$ and $\alpha = 1.278$ from Fig. 6. From (5.9b) and Fig. 11(a), the threshold for the Hopf bifurcation of the spike profile is $\tau_H = 94$. From (4.38), the oscillatory drift instability threshold is $\tau_{TW} = 39$. In Fig. 15(a) we show an oscillatory instability in the location of the spikes for $\tau > \tau_{TW}$. Although the spikes are initially located at $x_1(0) = -0.45$ and $x_2(0) = 0.5$, Fig. 15(a) shows that the instability eventually becomes a breathing-type instability as predicted by Conjecture 4.6. In Fig. 15(b) we show an oscillatory instability of the spike amplitudes v_m for spikes initially located at $x_1(0) = -x_2(0) = 0.5$. Although an asynchronous initial perturbation is given to the spike amplitudes, they are found to quickly synchronize as t increases.

Experiment 7: (Simultaneous Drift and Profile Instability) Next, we take $D = 0.25$, $A = 1.35$, $\varepsilon = 0.015$, and $k = 2$. For these values, we get $B = 1.286$ and $\alpha = 1.278$ from Fig. 6. From (5.9b) and Fig. 11(a), we estimate $\tau_H = 102$. From (4.38), we get $\tau_{TW} = 99.0$ and $\tau_{TW} = 66.9$ for a two and one-spike equilibrium solution, respectively. Therefore, when $k = 2$, the drift and profile instability thresholds are very close. We then choose $\tau = 90$ which is near these threshold values. The spikes are initially located at $x_1(0) = -0.45$ and $x_2(0) = 0.5$. In Fig. 16(a) we plot the spike trajectories, and in Fig. 16(b) we plot the spike amplitudes $v_{mj} \equiv v(x_j, t)$, where $x_j(t)$ is a local maximum of v. The second spike is annihilated

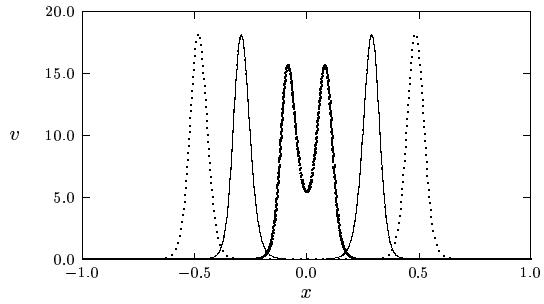

(a) v versus x

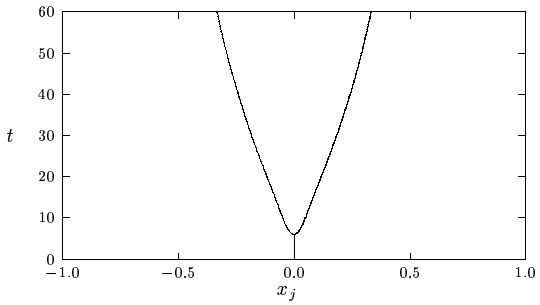

(b) t versus x_j

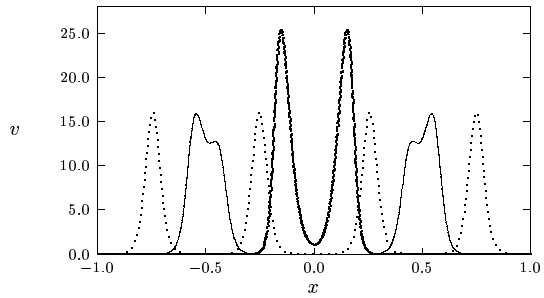

(c) v versus x_j

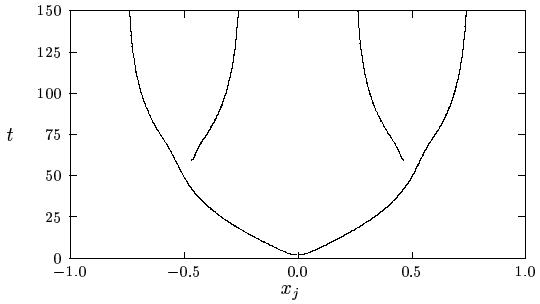

(d) t versus x_j

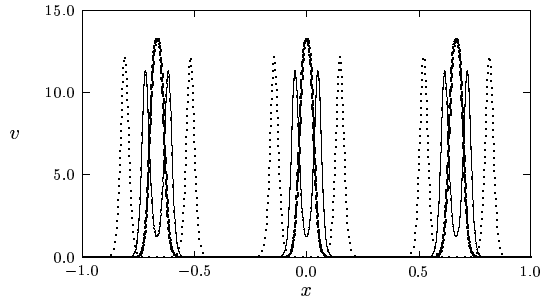

(e) v versus x_j

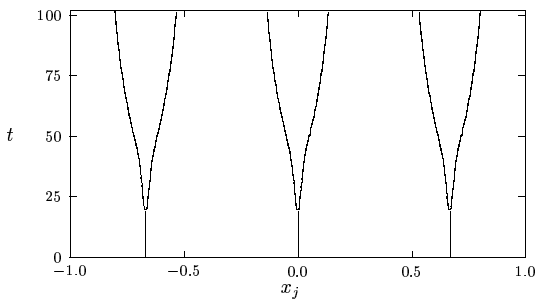

(f) t versus x_j

Figure 12: **Experiment 1** (top row): $\varepsilon = 0.02$, $k = 1$, $D = 0.75$, $A = 2.0$, and $\tau = 2.0$. Left figure: v at $t = 8.05$ (heavy solid curve), $t = 15$ (solid curve), and $t = 50.2$ (dashed curve). Right figure: t versus x_j with a pulse-split at $t \approx 6.0$. **Experiment 2** (middle row): $\varepsilon = 0.02$, $k = 1$, $D = 0.75$, $A = 3.0$, and $\tau = 2.0$. Left figure: v at $t = 10.0$ (heavy solid curve), $t = 61$ (solid curve), and $t = 100$ (dashed curve). Right figure: t versus x_j with pulse-splits at $t \approx 2.0$ and $t \approx 60.0$. **Experiment 3** (bottom row): $\varepsilon = 0.01$, $k = 3$, $D = 0.1$, $A = 1.9$, and $\tau = 2.0$. Left figure: v at $t = 10.0$ (heavy solid curve), $t = 50$ (solid curve), and $t = 100$ (dashed curve). Right figure: t versus x_j with a pulse-split at $t \approx 20.0$.

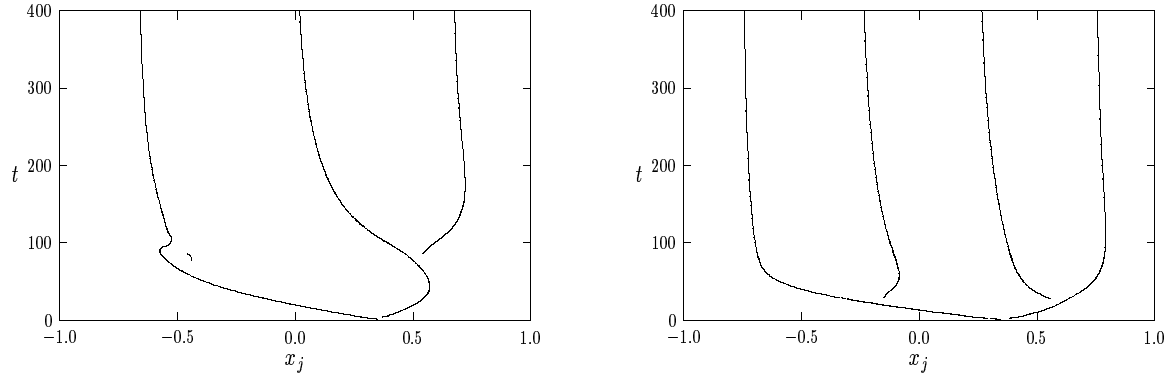

(a) t versus x_j: $A = 3.0$

(b) t versus x_j: $A = 4.0$

Figure 13: **Experiment 4:** t versus x_j for $\varepsilon = 0.02$, $k = 1$, $D = 0.75$, $\tau = 2.0$, and with an initial spike at $x_0(0) = 0.35$. Left figure: $A = 3.0$. Right figure: $A = 4.0$.

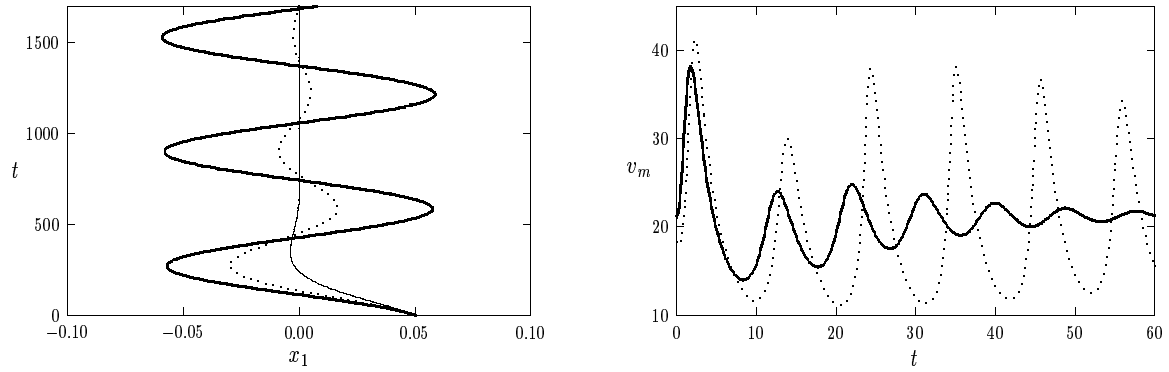

(a) t versus x_1

(b) v_m versus t

Figure 14: **Experiment 5:** Here $D = 0.25$, $A = 1.35$, $\varepsilon = 0.01$, and $k = 1$. Left figure: t versus x_1 for $\tau = 52$ (solid curve), $\tau = 65$ (dashed curve), and $\tau = 71$ (heavy solid curve). Right figure: v_m versus t for $\tau = 220$ (heavy solid curve) and $\tau = 235$ (dashed curve). Here v_m denotes the maximum value of $v(x, t)$.

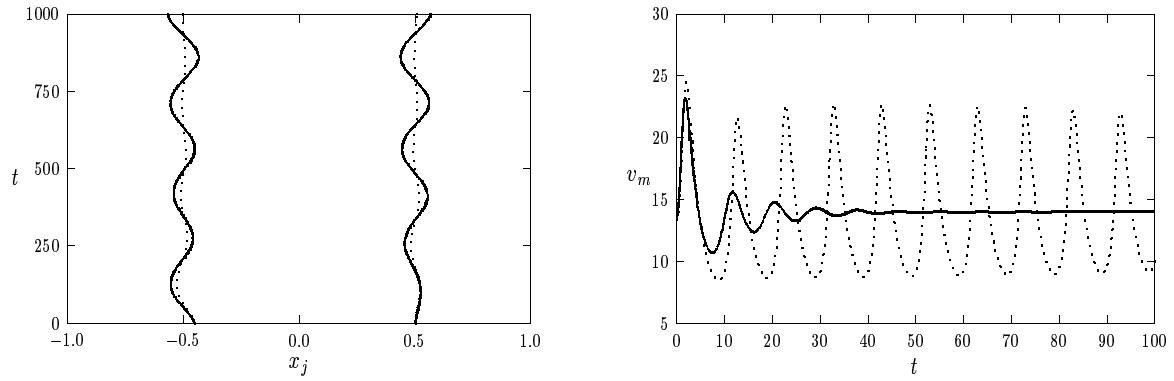

(a) t versus x_j

(b) v_m versus t

Figure 15: **Experiment 6:** Here $D = 0.1$, $A = 1.4$, $\varepsilon = 0.01$, and $k = 2$. Left figure: t versus x_j for $\tau = 55$ (heavy solid curve) and $\tau = 35$ (dashed curve). Right figure: v_m versus t for $\tau = 85$ (heavy solid curve) and $\tau = 105$ (dashed curve).

as a result of an oscillatory profile instability. The remaining spike then travels to the right and collapses against the right domain boundary at $t \approx 240$. Notice that since τ exceeds τ_{TW} for a one-spike solution, the final equilibrium state should not be a one-spike solution centered at the origin.

Experiment 8: (Large-Scale Drift Instability) Next, we take $D = 0.04$, $A = 1.5$, $\varepsilon = 0.0077$, and a single initial spike centered at the origin. From (2.26) we get $A_{p2} = 1.365$ and $A_{p4} = 1.588$. Therefore, for $\tau \ll O(\varepsilon^{-1})$, Conjecture 5.1 predicts a four-spike final equilibrium state. In the t versus x_j plot of Fig. 17(a) this is indeed observed when $\tau = 6.76$. However, for $\tau = 30$, Fig. 17(a) shows that the solution is a time-periodic two-spike state. For the intermediate value $\tau = 20$, we observe a time-periodic two-spike state that every half-period undergoes a brief splitting process before collapsing back to a two-spike solution. For this example, $\tau_{TW} = 35$ for a four-spike equilibrium solution, and $\tau_H = 64$.

Experiment 9: (Drift Instability, Three Spikes) Finally, we consider drift instabilities of a three-spike ($k = 3$) equilibrium solution when $D = 0.1$, $A = 1.6$, and $\varepsilon = 0.01$. From (4.38), the oscillatory drift instability threshold is $\tau_{TW} = 49.3$. From (5.9b), the profile instability threshold is $\tau_H = 94.5$. For $\tau = 75$, in Fig. 17(b) we show an oscillatory instability in the spike locations. Although the initial spike locations are $x_1(0) = -0.45$, $x_2(0) = 0.0$, and $x_3(0) = 0.50$, Fig. 17(b) shows that the instability eventually becomes a breathing-type instability as predicted by Conjecture 4.6.

7 Discussion

In this section we discuss the relationship between our results and those in the literature. We also list a few areas for further research.

First we summarize the comparison of our results with those of [28], [29], and [30]. Those works pertain

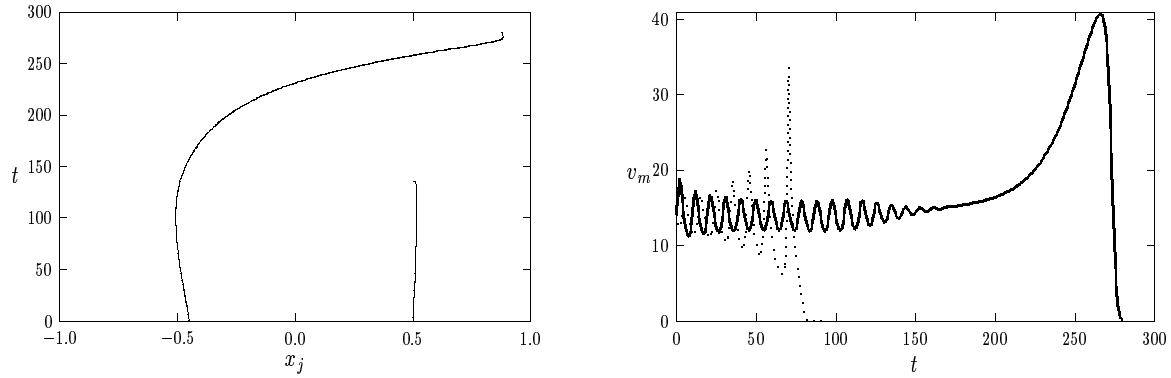

(a) t versus x_j (b) v_m versus t

Figure 16: **Experiment 7:** Here $D = 0.25$, $A = 1.35$, $\varepsilon = 0.015$, $k = 2$, and $\tau = 90$. Left figure: t versus x_j. Right figure: v_{m1} versus t (heavy solid curve) and v_{m2} versus t (dashed curve).

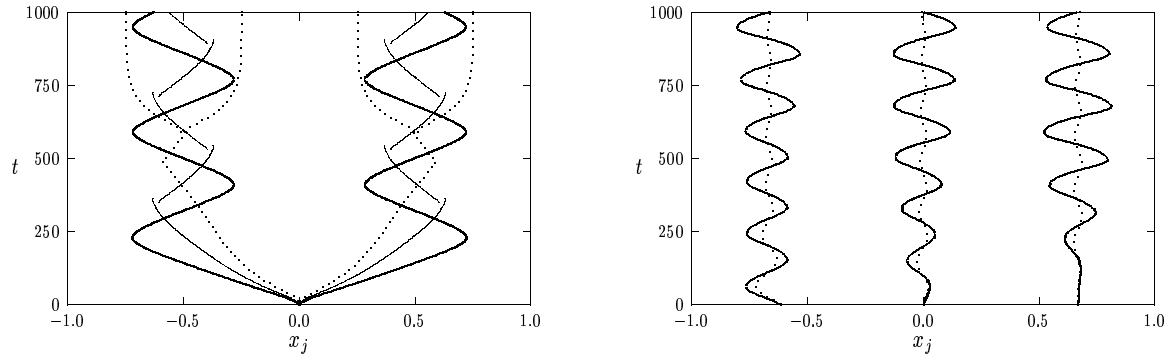

(a) t versus x_j (b) t versus x_j

Figure 17: Left figure: **Experiment 8:** Here $D = 0.04$, $A = 1.5$, $k = 1$, $\varepsilon = 0.0077$, with $\tau = 6.76$ (dashed curve), $\tau = 20.0$ (solid curve), and $\tau = 30.0$ (heavy solid curve). Right figure: **Experiment 9:** Here $D = 0.1$, $A = 1.6$, $k = 3$, $\varepsilon = 0.01$, with $\tau = 45$ (dashed curve) and $\tau = 75$ (heavy solid curve).

to a one-spike solution to (1.1) on the infinite line in the low feed-rate, intermediate, and pulse-splitting, regimes. This comparison, which has been made in appropriate places in this paper, in [20], and in [21], is transparent given that our starting point (1.1) is the dimensionless formulation of the GS model used in those works. In [29], the stability of a one-spike solution for the infinite-line problem was studied in the low-feed rate and intermediate regimes. For the low feed-rate and intermediate regimes, a favorable comparison of results is given in §3.4 of [20] and at the end of §4 in [20], respectively. In [28], the onset of a drift instability of a one-spike solution for the infinite-line problem in the intermediate regime was studied. This instability leads to a monotonic drift of the spike. In contrast, for the corresponding problem on the finite domain (of any fixed length) an oscillatory drift instability was found and analyzed in §5 of [22]. A precise and favorable comparison of results is given at the end of §5 of [22]. For a one-spike solution on the infinite line in the pulse-splitting regime $A = O(1)$, the core problem (2.10) was identified and solutions to it were computed numerically to identify the saddle-node value $A = 1.347$. Our far-field matching condition (2.11), which arises from inner-outer matching for a k-spike equilibrium, was not identified.

Next, we compare our results with those in [7] and [9], which are based on the following alternative dimensionless formulation of the GS model

$$V_T = \delta^2 V_{XX} - BV + UV^2\,, \qquad U_T = U_{XX} + A_{dgk}(1-U) - UV^2\,, \qquad 0 < X < L\,, \tag{7.1}$$

with $U_X = V_X = 0$ at $X = 0, L$, and $\delta \ll 1$. In terms of our variables D, ε, τ, and A, of (1.1), we have

$$D \equiv \frac{4}{A_{dgk}L^2}\,, \qquad \varepsilon^2 \equiv \frac{4\delta^2}{BL^2}\,, \qquad \tau \equiv \frac{B}{A_{dgk}}\,, \qquad A \equiv \frac{\sqrt{A_{dgk}}}{B}\,. \tag{7.2}$$

In [7] the scalings $A_{dgk} = \delta^2 a$ and $B = \delta^\beta b$, with $0 \le \beta \le 1$ were considered. Therefore, (7.2) becomes

$$A = \delta^{1-\beta}\frac{\sqrt{a}}{b}\,, \qquad \tau = \frac{\delta^{\beta-2}b}{a}\,, \qquad \frac{\varepsilon}{\sqrt{D}} = \delta^{2-\beta/2}\sqrt{\frac{a}{b}}\,. \tag{7.3}$$

In [7] solutions of a spatial period $\mathcal{T}$ are constructed. For a k-spike solution this determines L as $L = \mathcal{T}k$. In equation (2.10) of [7], the mode m of the periodic pattern is related to $\mathcal{T}$ by $m = (E^2+1)/(E^2-1)$, where $E = \exp(\mathcal{T}\delta\sqrt{a}/2)$. Using $L = \mathcal{T}k$, we can write m in terms of the notation in this paper as

$$m = \frac{1}{\tanh(\theta_0/k)}\,, \qquad \theta_0 = D^{-1/2}\,. \tag{7.4}$$

The pulse-splitting regime is where $A = O(1)$, and $\varepsilon A/\sqrt{D} \ll 1$. From (7.3) this corresponds to $\beta = 1$ and $\delta \ll 1$. For the infinite-line problem, it was proved using topological shooting in §6 of [7] that there exists a value B_d of B where there is a "disappearance bifurcation". The core problem (2.10) also appears as the leading-order terms in equation (2.9) of [9], without the far-field boundary condition (2.11). In §7.1 and §7.2 of [7], numerical methods, based on the numerical solution to a PDE, are used to compute the disappearance values B_d of B for the parameter value $a = 1$. For a one-spike solution on the infinite line in the pulse-splitting regime $\beta = 1$, numerical results for B_d for several δ are given in Table 1 of [7]. These results suggest that $B_d\delta^{-1} \equiv b_d$ is constant for small values of δ, although the constant limiting behavior of this quantity as $\delta \to 0$ is unspecified. In terms of our notation, if we set $\beta = 1$ and $a = 1$ in (7.3),

this suggests that the saddle-node value for A is independent of ε for $\varepsilon \to 0$. This corresponds to the core problem (2.10) on the infinite line where the saddle-node bifurcation is $A = 1.347$, as computed in [30].

The disappearance values B_d for periodic patterns of mode m were also computed numerically in §7.2 of [7]. The results were reported in Table 3 of [7] for $\delta^2 = 0.01$ and for the specific value $a = 1$ (i.e. $A_{dgk} = \delta^2$). The asymptotic theory of §6 of [7] showed that $b_d \equiv B_d \delta^{-1}$ is asymptotically independent of δ for $\delta \ll 1$. In addition, the numerical simulations of [7] strongly suggested that the product $mb_d(m)$ remains constant to leading order. The evidence for this numerically-based conjecture was given in the last three rows of Table 3 of [7]. In terms of our notation, we use (7.3) and (7.4) to calculate

$$b_d m = \frac{B_d m}{\delta} = \frac{\sqrt{A_{djk}}\, m}{A\delta} = \frac{\sqrt{a}\, m}{A} = \sqrt{a}\,[A \tanh(\theta_0/k)]^{-1} \ . \tag{7.5}$$

Compare the first and last expressions in (7.5) and set $a = 1$ as in [7]. It follows that the numerically-based conjecture of [7] that $b_d m$ is asymptotically constant is equivalent to the asymptotic constancy of $[A \tanh(\theta_0/k)]^{-1}$ as a function of k and ε. This is precisely the result that is established analytically in §2 in terms of an inner-outer matching of the core problem (2.10) to an appropriate far-field behavior. The common value for this constant is the saddle-node point for the core problem on the infinite line.

Pulse-splitting for (7.1), starting from an initial pulse at the origin, was computed numerically in Fig. 4 of [6] for $\delta^2 = 0.01$, $A_{dgk} = .01$, $B_d = 0.0474$, and $L = 100$, where a final equilibrium state of eight spikes was observed. Since $a = A_{dgk}\delta^{-2} = 1$, Table 3 of [7] is applicable, and using the numerical conjecture of [7] that $mb_d(m)$ is constant, the final state can be predicted from [7] . From (7.2), we have in terms of our notation that $\varepsilon = .00918$, $D = 0.04$, $A = 2.109$, $\tau = 4.74$, and so $\varepsilon A/\sqrt{D} = 0.097 \ll 1$. From (2.26), we get $A_{p4} < A < A_{p8}$. In addition, from (4.38), the drift instability threshold for an eight-spike equilibrium solution is $\tau_{TW} = 60.4 > \tau$. Therefore, Conjecture 5.1 also predicts an eight-spike final state. A similar direct comparison can be made for the pulse-splitting observed in Fig. 2b of [5] for the parameter set $A_{dgk} = .01$, $B = 0.0674$, $\delta^2 = 0.01$, and $L = 100$, where a four-spike final state was found. Since $A_{dgk}\delta^{-2} = a = 1$, Table 3 of [7] can be used to predict this final state. In terms of our notation, we calculate that $\varepsilon = 0.0077$, $D = 0.04$, $A = 1.483$, $\tau = 6.74$, and so $\varepsilon A/\sqrt{D} = .057$. From (2.26) and (4.38), we obtain $A_{p2} < A < A_{p4}$ and $\tau_{TW} = 37.4 > \tau$ for a four-spike equilibrium. Therefore, Conjecture 5.1 also predicts the four-spike final state. Experiments 1–3 in §6 are example of pulse-splitting, with no drift instabilities, corresponding to values $A_{dgk}\delta^{-2} \neq 1$ not considered in [7].

Next, we comment on previous results of [7] regarding the stability of k-spike (or equivalently) periodic patterns. In the intermediate regime, corresponding to $0 < \beta < 1$ in (7.3), the stability of these solutions with respect to the large eigenvalues is determined in terms of the NLEP given in (A.7) of Appendix A. The stability threshold in this regime, given in Proposition A.2, is asymptotically equivalent to the result first derived in equation (5.16) of [7]. However, as shown in Appendix A of [7], where $\beta < 1$ was assumed, this NLEP problem does not hold in the pulse-splitting regime where $\beta = 1$. In the pulse-splitting regime the more strongly coupled eigenvalue problem (5.1) holds when $\tau \ll O(\varepsilon^{-2})$. Notice that if we did formally set $\beta = 1$ in (A.4) of Appendix A of [7] and let $\delta \ll 1$, the resulting problem is equivalent to (5.1). The results in §6 provide the first numerical study of the spectrum of this eigenvalue problem. Likewise, the numerical computation for the large eigenvalue stability threshold with $\tau = O(\varepsilon^{-2})$ for (5.9) is new.

The study of drift instabilities in §5 in the pulse-splitting regime is new, and has not been reported in the literature. The analysis, which requires the development of correction terms (U_1, V_1) to the solution of the core problem (2.10), is very different than the study of §3 of [21] for the small eigenvalues in the low feed-rate and intermediate regimes.

There are some open problems related to the existence and stability of k-spike equilibria in the pulse-splitting regime $A = O(1)$. Two such problems are to prove rigorously the shape of the $B = B(\gamma)$ curve in Fig. 2(a), and to prove the formal results in Principal Results 2.2 and 3.2, that give the saddle-node values A_{pk} and the multi-bump solution structure along the secondary branch of the $B(\gamma)$ curve. Another open problem is to give a rigorous treatment of the stability properties of the primary and secondary solution branches with respect to both drift instabilities and instabilities associated with large eigenvalues.

For the GS model in the low feed-rate and intermediate regimes, and under the assumption of semi-strong spike interactions, there has been some previous studies of the dynamics of quasi-equilibrium patterns. For the infinite-domain problem, the dynamics and stability of a quasi-equilibrium two-spike pattern were first studied in [5] and [6]. The corresponding problem for the finite domain was considered in [41], where certain instability phenomena, which do not occur for the infinite-line problem, were discovered and analyzed. For the Gierer-Meinhardt model, related studies of spike dynamics in the semi-strong interaction regime for the finite-domain problem are given in [17] and [42]. For the weak interaction regime of [35], where both diffusivities are small and of the same order, spike dynamics for the GS and related models were studied in [10] and [11].

For the pulse-splitting regime $A = O(1)$, the quantitative formal asymptotic studies of [39] and [40] describe the slow motion of a spike and the mechanism by which a dynamic pulse-splitting event occurs. A more qualitative discussion of dynamic pulse-splitting is given in §5 of [6]. However, further research in this direction is needed. In particular, for a k-spike pattern with arbitrary initial spike locations, one would like to predict the times and locations where splitting events occur. Another open problem is to analyze large-scale oscillatory motion in the spike locations that occur after a drift instability is initiated. In these contexts, theoretical quantitative explanations for Experiments 4–9 would be interesting.

Another area where further research is needed in the context of, essentially, one-dimensional spike patterns, is to study the stability of stripes and rings in the two dimensional GS model with respect to both zig-zag instabilities associated with the small eigenvalues, and breakup instabilities of stripes into spots, which result from large eigenvalue instabilities. These stability properties should depend on the asymptotic range of the feed-rate parameter A. Work in this direction is given in [23], [27], and [22].

A The Intermediate Regime: $O(\varepsilon^{1/2}) \ll A \ll O(1)$

In this Appendix we summarize some prior existence and stability results for k-spike equilibrium solutions to (1.1) in the intermediate regime $O(\varepsilon^{1/2}) \ll A \ll O(1)$. Defining $\mathcal{A}$ by $A = \varepsilon^{1/2}\mathcal{A}$, we begin with the equilibrium result of [20] in the low feed-rate regime where $\mathcal{A} = O(1)$.

Principal Result A.1: *For $\varepsilon \to 0$, consider a k-spike equilibrium solution to (1.1) where the spikes have equal height. Then, when $\mathcal{A} > \mathcal{A}_{ke}$ there are two such solutions; the large solution u_-, v_-, and the small*

solution u_+, v_+. The v-component for such a solution satisfies

$$v_\pm \sim \frac{1}{\sqrt{\varepsilon}\mathcal{A}U_\pm}\sum_{j=1}^{k}\left(w\left[\varepsilon^{-1}(x-x_j)\right]+O\left(\frac{\varepsilon}{\mathcal{A}^2U_\pm^2D}\right)\right), \tag{A.1a}$$

where $w(y)$ satisfies (A.2) below and $x_j=-1+(2j-1)/k$ for $j=1,\ldots,k$. In the j^{th} inner region, where $|x-x_j|=O(\varepsilon)$, u is spatially constant to leading order, and satisfies $u_\pm \sim U_\pm\left[1+O\left(\varepsilon/(\mathcal{A}^2U_\pm^2D)\right)\right]$. Here $U_\pm$ and the saddle-node bifurcation value $\mathcal{A}_{ke}$ are given by

$$U_\pm=\frac{1}{2}\left[1\pm\sqrt{1-\frac{\mathcal{A}_{ke}^2}{\mathcal{A}^2}}\right], \qquad \mathcal{A}_{ke}\equiv\sqrt{\frac{12\theta_0}{\tanh(\theta_0/k)}}, \qquad \theta_0\equiv D^{-1/2}. \tag{A.1b}$$

The outer solution for u, valid for $|x-x_j|\gg O(\varepsilon)$ and $j=1,\ldots,k$, is given by

$$u_\pm \sim 1-\frac{(1-U_\pm)}{a_g}\sum_{j=1}^{k}G(x;x_j), \qquad a_g=\left[2\sqrt{D}\tanh(\theta_0/k)\right]^{-1}, \tag{A.1c}$$

where $G(x;x_j)$ is the Green's function satisfying (A.3) below.

This result is Principal Result 2.1 of [20]. In (A.1a), the spike profile $w(y)$ satisfies

$$w''-w+w^2=0, \quad -\infty<y<\infty; \qquad w\to 0 \quad \text{as} \quad |y|\to\infty; \quad w'(0)=0, \quad w(0)>0. \tag{A.2}$$

Hence, $w(y)=\frac{3}{2}\mathrm{sech}^2(y/2)$. In (A.1c), the Green's function $G(x;x_j)$ satisfies

$$DG_{xx}-G=-\delta(x-x_j), \qquad -1<x<1; \qquad G_x(\pm 1;x_j)=0. \tag{A.3}$$

In [20] and [21] the stability properties of (A.1) were examined in the low feed-rate regime $\mathcal{A}=O(1)$. Although the small solution v_+, u_+ was found to be unstable for any $\mathcal{A}>\mathcal{A}_{ke}$, the stability properties of the large solution v_-, u_- with respect to the large and small eigenvalues were found to depend intricately on the parameters D, τ, and k (see [20] and [21]).

Next, we consider the intermediate regime $O(1)\ll\mathcal{A}\ll O(\varepsilon^{-1/2})$, or equivalently $O(\varepsilon^{1/2})\ll A\ll O(1)$. For the remainder of this Appendix we re-label the large solution as v, u. For $\mathcal{A}\to\infty$, we get from (A.1b) that $U_-\sim\mathcal{A}_{ke}^2/4\mathcal{A}^2$. Substituting this relation into (A.1a) we obtain, with $A=\varepsilon^{1/2}\mathcal{A}$, that

$$v\sim\frac{\mathcal{A}\sqrt{D}}{3\sqrt{\varepsilon}\coth(\theta_0/k)}\sum_{j=1}^{k}w\left[\varepsilon^{-1}(x-x_j)\right], \qquad u\sim\frac{3\coth(\theta_0/k)}{\mathcal{A}^2\sqrt{D}}. \tag{A.4a}$$

For $\mathcal{A}\gg 1$, the corresponding outer solution from (A.1c) becomes

$$u_0(x)\sim 1-\frac{1}{a_g}\left(1-\frac{\mathcal{A}_{ke}^2}{4\mathcal{A}^2}\right)\sum_{j=1}^{k}G(x;x_j). \tag{A.4b}$$

Using (A.4a), we can calculate the norm $|v|_2$, defined in (1.3), in the intermediate regime as

$$|v|_2\sim\frac{\sqrt{6Dk}\mathcal{A}}{3\coth(\theta_0/k)}. \tag{A.5}$$

For the intermediate regime, the stability properties of the large solution, v and u, with respect to the large eigenvalues of order $\lambda = O(1)$ were first studied in [7]. An alternative approach to this stability analysis was given in §4 of [20]. As for the small eigenvalues of order $\lambda = O(\varepsilon^2)$, it was shown in Proposition 3.6 of [21] that a k-spike equilibrium solution is stable with respect to drift instabilities when $D = O(1)$ and $\tau = O(1)$. In contrast, the following result determines the stability threshold of k-spike equilibria with respect to the large $O(1)$ eigenvalues in the spectrum of the linearization:

Proposition A.2: *Let $\varepsilon \ll 1$, $D = O(1)$, and $O(1) \ll \mathcal{A} \ll O(\varepsilon^{-1/2})$. Then, the k-spike equilibrium large solution u, v, is stable with respect to the large eigenvalues when $\tau < \tau_H$, where*

$$\tau_H \sim \frac{\mathcal{A}^4 D}{9} \tanh^4(\theta_0/k)\, \tau_{0h} \left(1 - \frac{6\theta_0}{\mathcal{A}^2 \tanh(\theta_0/k)}\right)^2 + o(1)\,, \tag{A.6}$$

and $\tau_{0h} = 1.748$. As τ increases past τ_H, this solution loses its stability to a Hopf bifurcation.

This result is based on the spectral properties of the NLEP (nonlocal eigenvalue problem)

$$\Phi'' - \Phi + 2w\Phi - \frac{2w^2}{1+\sqrt{\tau_0 \lambda}} \left(\frac{\int_{-\infty}^{\infty} w\Phi\, dy}{\int_{-\infty}^{\infty} w\, dy}\right) = \lambda \Phi\,, \qquad -\infty < y < \infty\,; \qquad \Phi \to 0\,, \quad |y| \to \infty\,, \tag{A.7}$$

where τ_0 is a bifurcation parameter. This NLEP was first studied in [7] and [8], and an alternative approach was given in [20]. Proposition A.2 is written as Proposition 4.3 of [20]. It is asymptotically equivalent to the main stability result in equation (5.16) of [7] (see §5 of [20] for a precise comparison of results).

The scaling law for τ given in (A.6) for a Hopf bifurcation of the spike profile shows that $\tau = O(\mathcal{A}^4) \gg 1$ when $\mathcal{A} \gg 1$. Therefore, it is natural to seek drift instabilities of a k-spike equilibrium solution that occur when $\tau \gg 1$. For a one-spike solution, this was done in §5 of [21], where the following result was obtained:

Principal Result A.3: *Let $\varepsilon \ll 1$ and $\tau = O(\varepsilon^{-2})$. Then, an eigenvalue $\lambda = O(\varepsilon^2)$ associated with a drift instability of the one-spike large solution satisfies the nonlinear algebraic equation*

$$\lambda \sim \frac{2\varepsilon^2 s}{D} \left[\beta \tanh(\theta_0 \beta) \tanh\theta_0 - 1\right]\,, \qquad s \equiv \frac{1 - U_-}{U_-}\,, \qquad \beta \equiv \sqrt{1 + \tau\lambda}\,, \tag{A.8a}$$

where $\theta_0 = 1/\sqrt{D}$. In the intermediate parameter regime, where $O(1) \ll \mathcal{A} \ll O(\varepsilon^{-1/2})$, (A.8a) reduces to

$$\lambda \sim \frac{2\varepsilon A^2}{3\sqrt{D}} \tanh\theta_0 \left[\beta \tanh(\theta_0 \beta) \tanh\theta_0 - 1\right]\,, \qquad \beta \equiv \sqrt{1 + \tau\lambda}\,. \tag{A.8b}$$

Here $A = \varepsilon^{1/2}\mathcal{A}$. For $\delta \ll 1$, any unstable mode associated with the one-spike solution has the form

$$v \sim \frac{1}{\sqrt{\varepsilon}\mathcal{A} U_-} w(\varepsilon^{-1}[x - x_0(t)])\,, \qquad x_0 \sim -\varepsilon\delta e^{\lambda t}\,. \tag{A.8c}$$

The results (A.8c) and (A.8a) were given in (5.3b) and (5.5) of [21], respectively. The limiting result (A.8b) is obtained by using the asymptotic relation $s \sim 4\varepsilon^{-1} A^2/\mathcal{A}_{1e}^2$ that holds in the intermediate regime. The analysis of (A.8a) in [21] was based on introducing the new variables τ_d, ω, and ξ, defined by

$$\tau = \left(\frac{D}{2s\varepsilon^2}\right)\tau_d\,, \qquad \lambda = \left(\frac{2s\varepsilon^2}{D}\right)\omega\,, \qquad \xi = \tau_d \omega\,. \tag{A.9}$$

Substituting (A.9) into (A.8a), it follows that ξ satisfies $F(\xi) = 0$, where

$$F(\xi) \equiv \frac{\xi}{\tau_d} - G(\xi)\,, \qquad G(\xi) \equiv \beta \tanh\theta_0 \tanh(\theta_0\beta) - 1\,, \qquad \beta \equiv \sqrt{1+\xi}\,. \tag{A.10}$$

By analyzing the roots of (A.10), the following rigorous result was obtained in Proposition 5.2 of [21]:

Principal Result A.4: *Let $\varepsilon \ll 1$ and $\tau = O(\varepsilon^{-2})$, and consider the small eigenvalues with $\lambda = O(\varepsilon^2)$. Then, there is a complex conjugate pair of pure imaginary eigenvalues when $\tau_d = \tau_{dh}$. For any $\tau_d > \tau_{dh}$ there are exactly two eigenvalues in the right half-plane. These eigenvalues have nonzero imaginary parts when $\tau_{dh} < \tau_d < \tau_{dm}$, and they merge onto the positive real axis at $\tau_d = \tau_{dm}$. They remain on the positive real axis for all $\tau_d > \tau_{dm}$. The values τ_{dh} and τ_{dm} depend on D.*

Therefore, at the critical value $\tau = \tau_{TW}$ given by

$$\tau_{TW} = \frac{D}{2s\varepsilon^2}\tau_{dh}\,, \tag{A.11}$$

a pair of complex small eigenvalues enters the right half-plane through a Hopf bifurcation. This instability with respect to translations in the spike profile leads to oscillations in the spike-layer location. By comparing the thresholds for τ given in (A.11) and (A.6), it follows for $\varepsilon \ll 1$ that

$$\tau_H \ll \tau_{TW}\,, \quad \text{for} \quad O(\varepsilon^{1/2}) \ll A \ll A_{sw}\,; \qquad \tau_{TW} \ll \tau_H\,, \quad \text{for} \quad A_{sw} \ll A \ll O(1)\,, \tag{A.12}$$

where $A_{sw} \sim \left(0.0047 D\tau_{dh}\coth^2\theta_0\right)^{1/6}\mathcal{A}_{1e}\varepsilon^{1/6}$.

Therefore, as A is increased towards the pulse-splitting regime where $A = O(1)$, a traveling wave instability will occur before the Hopf bifurcation value associated with the spike profile. Such an idea was given in [29] for a one-spike solution on the infinite line, but where a monotonic drift instability was found. A key difference here is that for the finite domain, the traveling wave instability is oscillatory in nature and arises from a Hopf bifurcation (see §5 of [21]). Finally, if we set $\mathcal{A} = O(\varepsilon^{-1/2})$, or equivalently $A = O(1)$, in (A.11), (A.9), and (A.6), and then use $s = O(\varepsilon^{-1})$, we get the following scalings for drift and large eigenvalue instabilities in the pulse-splitting regime where $A = O(1)$:

$$\tau_{TW} = O(\varepsilon^{-1})\,, \quad \lambda = O(\varepsilon)\,; \qquad \tau_H = O(\varepsilon^{-2})\,, \quad \lambda = O(1)\,. \tag{A.13}$$

Acknowledgements

T. K. was supported by a PGS-B graduate scholarship from NSERC. M. J. W. thanks NSERC for their grant support, the IMS of the Chinese University of Hong Kong for their hospitality, and the University of Washington Applied Math group for the generous use of their computer facilities. J. W. thanks the support of RGC of Hong Kong and a direct grant from CUHK.

References

[1] E. Anderson et al. *LAPACK User's Guide: Third Edition*, SIAM Publications (1999).

[2] U. Ascher, R. Christiansen, R. Russell, *Collocation Software for Boundary Value ODE's*, Math. Comp., **33**, (1979), pp. 659-679.

[3] E. J. Crampin, P. K. Maini, *Reaction-Diffusion Models for Biological Pattern Formation*, Methods and Appl. of Analysis, **8**, No. 2, (2001), pp. 415-428.

[4] M. Del Pino, M. Kowalczyk, X. Chen, *The Gierer Meinhardt System: The Breaking of Homoclinics and Multi-Bump Ground States*, Commun. Contemp. Math., **3**, No. 3, (2001), pp. 419-439.

[5] A. Doelman, W. Eckhaus, T. J. Kaper, *Slowly Modulated Two-Pulse Solutions in the Gray-Scott Model I: Asymptotic Construction and Stability*, SIAM J. Appl. Math., **61**, No. 3, (2000), pp. 1080-1102.

[6] A. Doelman, W. Eckhaus, T. J. Kaper, *Slowly Modulated Two-Pulse Solutions in the Gray-Scott Model II: Geometric Theory, Bifurcations, and Splitting Dynamics*, SIAM J. Appl. Math., **61**, No. 6, (2000), pp. 2036-2061.

[7] A. Doelman, R. A. Gardner, T. J. Kaper, *Stability Analysis of Singular Patterns in the 1D Gray-Scott Model: A Matched Asymptotics Approach*, Physica D, **122**, No. 1-4, (1998), pp. 1-36.

[8] A. Doelman, R. A. Gardner, T. Kaper, *A Stability Index Analysis of 1-D Patterns of the Gray Scott Model*, Memoirs of the AMS, **155**, No. 737, (2002).

[9] A. Doelman, T. J. Kaper, P. Zegeling, *Pattern Formation in the One-Dimensional Gray-Scott Model*, Nonlinearity, **10**, No. 2, (1997), pp. 523-563.

[10] S. Ei, Y. Nishiura, K. Ueda, 2^n *Splitting or Edge Splitting?: A Manner of Splitting in Dissipative Systems*, Japan. J. Indust. Appl. Math., **18**, (2001), pp. 181-205.

[11] S. Ei, *The Motion of Weakly Interacting Pulses in Reaction-Diffusion Systems*, J. Dynam. Differential Equations, **14**, No. 1, (2002), pp. 85-137.

[12] T. Erneux, E. L. Reiss, L. J. Holden, M. Georgiou, *Slow Passage Through Bifurcation and Limit Points. Asymptotic Theory and Applications*, Dynamic Bifurcations (Luminy 1990), Lecture Notes in Math., **1493**, Springer, Berlin, (1991), pp. 14-28.

[13] A. Gierer, H. Meinhardt, *A Theory of Biological Pattern Formation*, Kybernetik, **12**, (1972), pp. 30–39.

[14] G. Goldsztein, F. Broner, S. H. Strogatz, *Dynamical Hysteresis Without Static Hysteresis: Scaling Laws and Asymptotic Expansions*, SIAM J. Appl. Math., **57**, No. 4, (1997), pp. 1163-1187.

[15] P. Gray, S. K. Scott, *Autocatalytic Reactions in the Isothermal, Continuous Stirred Tank Reactor: Oscillations and Instabilities in the System* $A + 2B \to 3B$, $B \to C$, Chem. Eng. Sci. **39**, (1984), pp. 1087-1097.

[16] T. Ikeda, Y. Nishiura, *Pattern Selection for Two Breathers*, SIAM J. Appl. Math., **54**, No. 1, (1994), pp. 195-230.

[17] D. Iron, M. J. Ward, *The Dynamics of Multi-Spike Solutions to the One-Dimensional Gierer-Meinhardt Model*, SIAM J. Appl. Math., **62**, No. 6, (2002), pp. 1924-1951.

[18] D. Iron, M. J. Ward, J. Wei, *The Stability of Spike Solutions to the One-Dimensional Gierer-Meinhardt Model*, Physica D, **150**, No. 1-2, (2001), pp. 25-62.

[19] B. S. Kerner, V. V. Osipov, *Autosolitions: A New Approach to Problem of Self-Organization and Turbulence*, Kluwer Academic Publishers, Dordrecht, (1994).

[20] T. Kolokolnikov, M. Ward, J. Wei, *The Stability of Spike Equilibria in the One-Dimensional Gray-Scott Model: The Low Feed-Rate Regime*, accepted, Studies in Appl. Math., (2004), (49 pages).

[21] T. Kolokolnikov, M. Ward, J. Wei, *Slow Translational Instabilities of Spike Patterns in the One-Dimensional Gray-Scott Model*, submitted, Disc. Contin. Dyn. Sys. Series B, (2005).

[22] T. Kolokolnikov, M. Ward, J. Wei, *Zigzag and Breakup Instabilities of Stripes and Rings in the Two Dimensional Gray-Scott Model*, submitted, Europ. J. Appl. Math., (2005).

[23] T. Kolokolnikov, J. Wei, *On Ring-Like Solutions for the Gray-Scott Model: Existence, Instability, and Self-Replicating Regimes*, to appear, Europ. J. Appl. Math., (2004).

[24] K. J. Lee, W. D. McCormick, J. E. Pearson, H. L. Swinney, *Experimental Observation of Self-Replicating Spots in a Reaction-Diffusion System*, Nature, **369**, (1994), pp. 215-218.

[25] K. J. Lee, H. L. Swinney, *Lamellar Structures and Self-Replicating Spots in a Reaction-Diffusion System*, Phys. Rev. E., **51**, (1995), pp. 1899-1915.

[26] M. Mimura, N. Nishiura, *Layer Oscillations in Reaction Diffusion Systems*, SIAM J. Appl. Math., **49**, No. 2, (1989), pp. 481-514.

[27] D. Morgan, T. Kaper, *Axisymmetric Ring Solutions of the Two Dimensional Gray-Scott Model and Their Destabilization into Spots*, Physica D, **192**, No. 1-2, (2004), pp. 33-62.

[28] C. Muratov, V. V. Osipov, *Traveling Spike Auto-Solitons in the Gray-Scott Model*, Physica D, **155**, No. 1-2, (2001), pp. 112-131.

[29] C. Muratov, V. V. Osipov, *Stability of the Static Spike Autosolitons in the Gray-Scott Model*, SIAM J. Appl. Math., **62**, No. 5, (2002), pp. 1463-1487.

[30] C. Muratov, V. V. Osipov, *Static Spike Autosolitons in the Gray-Scott Model*, J. Phys. A: Math Gen. **33**, (2000), pp. 8893-8916.

[31] NAG Fortran library Mark 17, routine D03PCF, Numerical Algorithms Group Ltd., Oxford, United Kingdom (1995).

[32] Y. Nishiura, H. Fujii, *Stability of Singularly Perturbed Solutions to Systems of Reaction-Diffusion Equations*, SIAM J. Math. Anal., **18**, (1987), pp. 1726-1770.

[33] Y. Nishiura, *Global Bifurcational Approach to the Onset of Spatio-Temporal Chaos in Reaction-Diffusion Systems*, Methods and Appl. of Analysis, **8**, No. 2, (2001), pp. 321-332.

[34] Y. Nishiura, T. Teramoto, K. Ueda, *Scattering and Separators in Dissipative Systems*, Phys. Rev. E., **67**, No. 5, 56210, (2003).

[35] Y. Nishiura, D. Ueyama, *A Skeleton Structure of Self-Replicating Dynamics*, Physica D, **130**, No. 1-2, (1999), pp. 73-104.

[36] Y. Nishiura, D. Ueyama, *Spatio-Temporal Chaos for the Gray-Scott Model*, Physica D, **150**, No. 3-4, (2001), pp. 137-162.

[37] J. E. Pearson, *Complex Patterns in a Simple System*, Science, **216**, (1993), pp. 189-192.

[38] V. Petrov, S. K. Scott, K. Showalter, *Excitability, Wave Reflection, and Wave Splitting in a Cubic Autocatalysis Reaction-Diffusion System*, Phil. Trans. Roy. Soc. Lond., Series A, **347**, (1994), pp. 631-642.

[39] W. N. Reynolds, S. Ponce-Dawson, J. E. Pearson, *Dynamics of Self-Replicating Patterns in Reaction-Diffusion Systems*, Phys. Rev. Lett., **72**, (1994), pp. 2797-2800.

[40] W. N. Reynolds, S. Ponce-Dawson, J. E. Pearson, *Dynamics of Self-Replicating Spots in Reaction-Diffusion Systems*, Phys. Rev. E, **56**, No. 1, (1997), pp. 185-198.

[41] W. Sun, M. J. Ward, R. Russell, *The Slow Dynamics of Two-Spike Solutions for the Gray-Scott and Gierer-Meinhardt Systems: Competition and Oscillatory Instabilities*, submitted, SIAM J. App. Dyn. Systems, April (2004).

[42] W. Sun, T. Tang, M. J. Ward, J. Wei, *Numerical Challenges for Resolving Spike Dynamics for Two Reaction-Diffusion Systems*, Studies in Appl. Math., **111**, (2003), pp. 41-84.

[43] D. Ueyama, *Dynamics of Self-Replicating Patterns in the One-Dimensional Gray-Scott Model*, Hokkaido Math J., **28**, No. 1, (1999), pp. 175-210.